Published in final edited form as:
J Neurosci. 2012 June 13; 32(24): 8158–8172. doi:10.1523/JNEUROSCI.0251-12.2012.

CDK-5 regulates the polarized trafficking of neuropeptide-containing dense-core vesicles in *C. elegans* motor neurons

Patricia R. Goodwin[1,2], **Jennifer M. Sasaki**[1,2], and **Peter Juo**[1,3]

[1]Department of Molecular Physiology and Pharmacology, Sackler School of Graduate Biomedical Sciences, Tufts University School of Medicine, 150 Harrison Avenue, Boston, MA 02111

[2]Graduate Program in Neuroscience, Sackler School of Graduate Biomedical Sciences, Tufts University School of Medicine, 150 Harrison Avenue, Boston, MA 02111

Abstract

The polarized trafficking of axonal and dendritic proteins is essential for the structure and function of neurons. Cyclin-dependent kinase-5 (CDK-5) and its activator CDKA-1/p35 regulate diverse aspects of nervous system development and function. Here, we show that CDK-5 and CDKA-1/p35 are required for the polarized distribution of neuropeptide-containing dense-core vesicles (DCVs) in *C. elegans* cholinergic motor neurons. In *cdk-5* or *cdka-1*/p35 mutants, the predominantly axonal localization of DCVs containing INS-22 neuropeptides was disrupted and DCVs accumulated in dendrites. Time-lapse microscopy in DB class motor neurons revealed decreased trafficking of DCVs in axons and increased trafficking and accumulation of DCVs in *cdk-5* mutant dendrites. The polarized distribution of several axonal and dendritic markers, including synaptic vesicles, was unaltered in *cdk-5* mutant DB neurons. We found that microtubule polarity is plus-end out in axons and predominantly minus-end out in dendrites of DB neurons. Surprisingly, *cdk-5* mutants had increased amounts of plus-end-out microtubules in dendrites, suggesting that CDK-5 regulates microtubule orientation. However, these changes in microtubule polarity are not responsible for the increased trafficking of DCVs into dendrites. Genetic analysis of *cdk-5* and the plus-end-directed axonal DCV motor *unc-104*/KIF1A suggest that increased trafficking of UNC-104 into dendrites cannot explain the dendritic DCV accumulation. Instead, we found that mutations in the minus-end-directed motor cytoplasmic dynein, completely block the increased DCVs observed in *cdk-5* mutant dendrites without affecting microtubule polarity. We propose a model where CDK-5 regulates DCV polarity by both promoting DCV trafficking in axons and preventing dynein-dependent DCV trafficking into dendrites.

Introduction

Neurons are highly polarized cells with molecularly and functionally distinct dendritic and axonal compartments that ensure the directional flow of information. The establishment and maintenance of neuronal polarity requires strict mechanisms for the polarized sorting of pre- and postsynaptic proteins to axons and dendrites, respectively.

Cyclin-dependent kinase-5 (CDK-5) and its cyclin-like activator CDKA-1/p35 regulate diverse cellular functions in the nervous system, such as cell migration, axon outgrowth, and synaptic transmission (Cheung et al., 2006; Dhavan and Tsai, 2001). In particular, CDK-5 regulates the transport of membrane-bound organelles in cultured squid and rodent axons

[3]Corresponding author Peter Juo, Ph.D. Department of Molecular Physiology and Pharmacology, Tufts University School of Medicine, 150 Harrison Avenue, Boston, MA 02111, Tel: 617-636-3950, Fax: 617-636-0445, peter.juo@tufts.edu.

(Morfini et al., 2004; Pandey and Smith, 2011; Ratner et al., 1998) and was recently shown to promote polarized trafficking in *C. elegans* (Ou et al., 2010). Ou et al. showed that CDK-5 and another cyclin-dependent kinase, PCT-1, regulate the polarized trafficking of synaptic vesicles (SVs) in cholinergic motor neuron axons by inhibiting retrograde trafficking by the minus-end-directed microtubule motor dynein. Interestingly, this polarity mechanism was cell-type specific, because these kinases are required for the polarized trafficking of SVs in DA class motor neurons but, surprisingly, not in related DB class motor neurons (Ou et al., 2010). This research raises several interesting questions regarding whether CDK-5 has a broader role in regulating neuronal polarity: (1) Does CDK-5 affect the polarized trafficking of other cargo, such as secreted cargo? (2) Does CDK-5 regulate fundamental aspects of polarity such as microtubule orientation? and (3) Does CDK-5 regulate any aspect of neuronal polarity in DB motor neurons?

We addressed these questions by investigating the role of CDK-5 in regulating the polarized trafficking of neuropeptides in motor neurons in *C. elegans*. Much research has focused on the molecular mechanisms involved in the polarized trafficking of transmembrane proteins to axons and dendrites, and SV precursors to presynaptic sites (Horton and Ehlers, 2003; Ou and Shen, 2010). Less is known about the polarized trafficking mechanisms by which neurons target secreted cargo, like neuropeptide-filled dense-core vesicles (DCVs), to their sites of release. DCVs carry diverse cargo such as neuropeptides, neurotrophins and peptide hormones, and are involved in modulating synaptic transmission, plasticity and behavior (Lessmann and Brigadski, 2009; Li and Kim, 2008). Unlike SVs, which are recycled and refilled with neurotransmitter at the presynaptic terminal, DCVs are packaged with their protein cargo at the *trans*-golgi network in the cell body, undergo a complex biogenesis process, and must be continuously transported to their sites of release (Borgonovo et al., 2006; Dikeakos and Reudelhuber, 2007; Edwards et al., 2009; Sumakovic et al., 2009). In addition, depending on their cargo, DCVs can be targeted to release sites in axons and/or dendrites (Fisher et al., 1988; Landry et al., 2003; Lessmann and Brigadski, 2009). However, little is known about the mechanisms that control DCV targeting to either subcellular compartment.

Here, we show that CDK-5 is required for the polarized trafficking of DCVs in DA and DB motor neurons, and propose a model where CDK-5 both promotes DCV trafficking in axons and prevents dynein-dependent DCV trafficking into dendrites.

Materials and Methods

Strains

Strains were maintained on OP50 *E. coli* at 20°C as described by Brenner et al (1974). The following strains were used in this study: N2 Bristol, *nuIs195 (Punc-129::ins-22::venus), ceIs72(Punc-129::ida-1::gfp), nuIs165 (Punc-129::unc-10::gfp), nuIs174 (Punc-129::gfp::rab-3), pzEx77 (Punc-17::cdk-5), pzEx107(Punc-17::cdk-5(D144N)), pzEx114(Punc-129::cdka-1), pzEx140(Punc-129::cdk-5), pzEx133(Punc-129::fbn-1::gfp), pzEx156(Punc-129::ebp-1::gfp), pzEx220(Punc-129::gfp::dli-1), yuEx46(Punc-129::unc-9::gfp; Punc-129::mCherry)*(gift from Lars Dreier), *cdk-5(gm336), cdk-5(ok626), cdka-1(gm335), unc-10(e102), unc-104(e1265), dhc-1(js319), dli-1(ku266).* The *cdk-5* allele *gm336* is a predicted null mutation and consists of a 760 bp deletion that eliminates the start codon as previously described (Juo et al., 2007). The *ok626* allele is also a predicted null mutation that consists of a 1.6kb deletion that eliminates the *cdk-5* start codon but also deletes part of a neighboring gene T27E9.4.

Constructs, transgenes, and germline transformation

Plasmids were generated using standard cloning techniques and details are available upon request. *Punc-129::cdk-5* (FJ#55) and *Punc-129::cdka-1* (FJ#56) were generated by subcloning *cdk-5* from *pV6::cdk-5* (KP#1414) and *cdka-1* from *pV6::cdka-1* (KP#1413) into the *Punc-129* expression vector KP#1271. The *unc-129* promoter contains a 2644 bp fragment upstream of the *unc-129* start codon that was amplified by PCR using the following primers (ODS276: 5′ GGGGGGGCATGCGGAAACATGATATCGACGGAC 3′ and ODS277: 5′ GGGGGGGGATCCCTTGCTTGCTCTTCCAATTTTCC 3′)(Sieburth et al., 2005). Wild-type and kinase-dead *cdk-5* were subcloned from *pV6::cdk-5* (KP#1414) and *pV6::cdk-5(D144N)* (KP#1415), respectively, and put under the control of the *unc-17* promoter. The *unc-17* promoter consists of a 3213 bp fragment of the *unc-17* 5′UTR that was amplified with the following PCR primers (UNC17-FWD: 5′ TTCACATCCCCCGAAATTTCC 3′ and UNC17-REV: 5′ GACTTTTAATTTATAAAATCACATTTTG 3′) The *fbn-1* and *ebp-1* open reading frame were obtained by RT-PCR from wild-type cDNA and subcloned under the control of the *unc-129* promoter. NotI sites were introduced at the C-termini of both genes and used to insert GFP to create *Punc-129::FBN-1::GFP* (FJ#57) and *Punc-129::ebp-1::GFP* (FJ#62). GFP::DLI-1 was subcloned from *Pjkk-1::GFP::DLI-1* (gift from Naoki Hisamoto) and put under the control of the *unc-129* promoter to create *Punc-129::GFP::DLI-1* (FJ#68). Transgenic strains were generated by microinjection of various plasmids at the following concentrations: 50 ng/μl for *Punc-17::cdk-5(wt), Punc-17::cdk-5(D144N), Punc-129::cdk-5,* and *Punc-129::cdka-1*, 25ng/μl for *Punc-129::fbn-1::gfp* and *Punc-129::gfp::dli-1*, and 1ng/μL for *Punc-129::ebp-1::gfp*. Plasmids were injected with various co-injection markers: *Pttx-3::dsred*, *Pmyo-2::nls::gfp*, or *Pmyo-2::nls::mcherry.*

Fluorescent Microscopy and Quantification

All imaging was performed using a Zeiss M1 Axioimager microscope. For all experiments, except for time-lapse imaging, young adult hermaphrodites were immobilized with 30mg/mL 2,3-Butanedione monoxamine (Sigma Aldrich) for 5–7 minutes and mounted on 2% agarose pads prior to imaging. Images were taken using a Zeiss 100X planapo objective (NA 1.4) and an Orca-ER (Hamamatsu) CCD camera. Maximum intensity projections of Z-series stacks and line scans of fluorescent puncta were obtained using Metamorph (v7.1) software (Molecular Devices). For quantitative analyses of fluorescent ventral and dorsal nerve cord puncta, maximum intensity projections of Z series stacks (total depth 1μm) were made. Exposure settings and gain were set to fill the 12-bit dynamic range without saturation and were constant for all images of a given fluorescent marker. FluoSphere yellow-green fluorescent beads (Invitrogen) were imaged daily to correct for day-to-day variation in microscope light bulb intensity. All images (unless stated otherwise) were taken from animals oriented with the dorsal or ventral nerve cord up and laterally oriented animals were excluded. Images containing mobile INS-22::Venus puncta were excluded from analysis.

The *unc-129* promoter drives expression of genes in a subset of DA motorneurons, which have processes projecting towards the head, and a subset of DB neurons, which project towards the tail (Fig. 1). DA6 is the most posterior DA neuron with visible expression of fluorescent markers driven by the *unc-129* promoter, thus all fluorescent signal posterior to the DA6 neuron is derived only from DB neurons. To isolate only DB axons in the dorsal nerve cord (DNC), we drew line scans along the DNC posterior to the site of DA6 commissure entry. To isolate only DB dendrites in the ventral nerve cord (VNC), we drew line scans posterior to the DA6 cell body. In our analysis of microtubule orientation in the DB axons (Fig. 4), we find that >95% of microtubules in this area of the DNC are oriented in the same direction, suggesting that this section of the nerve cord is not contaminated by fluorescent signal from DA neurons. To image INS-22::Venus primarily in DA neurons, we

imaged anterior to the DA3 cell body for the VNC and anterior to the site of DA3 commissure entry into the DNC (DA rich region indicated in Fig. 1). In most animals, there was no expression of fluorescent markers in any DB neurons in this region, however in ~20% of wild type animals there was weak expression of INS-22::Venus in the DB3 cell body, suggesting that the vast majority of fluorescent signal in this section of the nerve cord is derived from DA neurons, with a small amount of signal from DB neurons.

Line scans of nerve cord puncta were generated using MetaMorph (v6.0) and were then analyzed in Igor Pro (v5) using custom written software as previously described (Burbea et al., 2002). Puncta intensity and density were calculated for each image. Puncta intensity is the fractional increase in peak fluorescence of each puncta over fluorescent bead intensity for that date. Puncta density is the average number of puncta per 10 μm of nerve cord. For DB6 cell body imaging, lateral and ventral up animals were imaged, and Z stacks were taken to a depth of 2 μm. Average fluorescence of three fluorescent patches per cell body was measured using Metamorph software, then corrected for daily bead values and analyzed in Microsoft Excel.

For GFP::DLI-1 imaging, lateral and ventral up animals were imaged, and Z stacks were taken to a depth of 1 μm. The fluorescence of the most posterior GFP::DLI-1 punctum in the VNC was measured using Metamorph software, then corrected for daily bead values and analyzed in Microsoft Excel.

Changes in puncta intensity and density were analyzed for statistical significance using the Students' *t* test for two genotype comparisons and the Tukey-Kramer test for multiple genotype comparisons.

Time-lapse microscopy

For time-lapse microscopy of INS-22::Venus, young adult worms were paralyzed in 1.5 mM Levamisol (Sigma) dissolved in M9 buffer for 6 to 7 minutes. Animals were mounted on 2% agarose pads containing 1.5 mM Levamisol. Time-lapse images were taken at 4 Hz speed for 20 seconds and saved as a Z series. For dendritic INS-22::Venus, movies were taken of DB6 dendrites in a region of the VNC between the DA6 and DB7 cell bodies (Fig. 1). Because DB processes project posteriorly, all movements towards the tail were designated anterograde and all movements towards the head were designated retrograde. For axon commissure time-lapse imaging, movies were taken of DB6 commissures in ventral-up and ventrolaterally oriented animals, with line scans drawn from the DB6 cell body to the last in-focus INS-22::Venus punctum. These scans were used to generate kymographs in MetaMorph (v7.1). INS-22::Venus puncta direction of movement and velocity were calculated by tracing these kymographs. Each mobile puncta was traced during its longest uninterrupted period of movement. Puncta were defined as mobile if they moved distances greater than twice their own width and at velocities greater than 0.1 μm/s. Puncta that changed direction were traced for both directions for analysis of puncta velocity and direction of movement, but were only counted once for analysis of total puncta. Kymograph traces were compiled for analysis in Microsoft Excel. Average anterograde and retrograde velocity, and the number of stationary, anterogradely, and retrogradely moving puncta were calculated for each kymograph (i.e. worm) and these data were compiled for each genotype and analyzed in Microsoft Excel. For two genotype comparisons, Student's *t* tests were used to detect differences between genotypes. For greater than two genotype comparisons, the Tukey-Kramer test was used to detect differences between genotypes. The Kolmogorov-Smirnov (KS) test was used for puncta velocity comparisons.

Kymograph analysis using Metamorph software was also used to measure the fluorescence intensity of mobile INS-22::Venus puncta in dendrites. The maximum fluorescence intensity

of each mobile punctum was measured at the t=0 time point of each kymograph, to minimize the effects of photobleaching. Maximum intensity measurements were analyzed using Microsoft Excel and IgorPro (v5). Occasionally, mobile INS-22::Venus puncta were observed to undergo a splitting event, where a single punctum divides into two separate puncta during the time-lapse movie. While these events are rare, it suggests that a mobile punctum may represent more than one DCV. For this reason, splitting puncta were excluded from mobile INS-22::Venus fluorescence intensity analyses in order to enrich for puncta representing single DCVs.

For time-lapse microscopy of EBP-1 movement, animals were paralyzed in 2mM Levamisol dissolved in M9 for 8 to 9 minutes and mounted on a 2% agarose pad containing 2mM Levamisol. In the VNC, line scans were drawn in DB6 or DB7 dendrites from the DA6 or DB7 cell body towards the tail. In the DNC, line scans were drawn towards the tail in DB6 axons immediately posterior to the site of DA6 commissure entry into the nerve cord (DB only region is indicated on Fig. 1). Time-lapse images were taken at a speed of 4Hz for 25s. EBP-1::GFP direction of movement and velocity were calculated by tracing puncta in these kymographs. Only puncta that could be followed for 2s or more were included. Occasionally, oscillating puncta were visible, consistent with reports from (Stepanova et al., 2003), and these puncta were excluded from analysis. Direction of movement and velocity of EBP-1::GFP puncta were analyzed using Microsoft Excel. Changes in percentages of plus-end and minus-end out microtubules were compared across genotypes using Chi-squared analysis, with a Yates' correction employed for two genotype comparisons (i.e. 2×2 contingency tables).

Results

CDK-5 regulates the polarized distribution of DCVs in DB motor neurons

We investigated whether CDK-5 regulates the polarized trafficking of neuropeptide-containing DCVs in DA and DB cholinergic motor neurons in *C. elegans*. Each DA/DB neuron has a simple polarized morphology consisting of a cell body and a single dendrite in the ventral nerve cord (VNC), where it receives inputs, and a single axon in the dorsal nerve cord (DNC), where it makes synapses onto muscle and GABAergic motor neurons (Fig. 1 and 2*A,D*)(White et al., 1986). DA class motor neurons extend their processes towards the anterior and are involved in backward locomotion, whereas DB class motor neurons extend their processes towards the posterior and are involved in forward locomotion (Chalfie et al., 1985; Haspel et al., 2010; White et al., 1986). We used the *unc-129* promoter to drive expression of fluorescent markers in a subset of DA and DB motor neurons (Fig. 1*A*) (Sieburth et al., 2005; Sieburth et al., 2007). Figure 1B shows an image of the VNC illustrating specific DA and DB cell bodies and processes that express soluble mCherry under the control of the *unc-129* promoter. In this study, we imaged specific regions of the VNC (dendrites) and DNC (axons) in order to separate fluorescent signals from either DA or DB motor neurons (Figure 1).

To visualize DCVs in DA and DB motor neurons, we expressed a Venus-tagged neuropeptide, insulin-like protein 22 (INS-22::Venus) under the control of the *unc-129* promoter (Sieburth et al., 2005; Sieburth et al., 2007). We chose the neuropeptide *ins-22* because it is expressed in ventral cord motor neurons and has been implicated in regulating synaptic transmission at the *C. elegans* NMJ (Pierce et al., 2001; Sieburth et al., 2005). In addition, INS-22::Venus has been well characterized as a DCV marker (Ch'ng et al., 2008; Edwards et al., 2009; Sieburth et al., 2005; Sieburth et al., 2007). In wild-type animals, INS-22::Venus has a highly polarized subcellular distribution where it is largely excluded from the motor neuron dendrites and is localized in a punctate manner in the motor neuron axons (Fig. 2*A–F*)(Sieburth et al., 2007). INS-22::Venus co-localizes with and adjacent to

synaptobrevin in the axon (Sieburth et al., 2007), consistent with electron microscopy findings which indicate that DCVs are broadly distributed at presynaptic sites and only slightly enriched at the active zone (Hammarlund et al., 2008). Trafficking of INS-22::Venus to the axon requires the anterograde kinesin motor UNC-104/KIF1A, as has been shown for several other DCV markers and endogenous neuropeptides (Barkus et al., 2008; Jacob and Kaplan, 2003; Sieburth et al., 2005; Sieburth et al., 2007; Zahn et al., 2004).

To investigate whether CDK-5 regulates the polarized distribution of DCV cargo in *C. elegans*, we analyzed the distribution of INS-22::Venus-containing DCVs in DA and DB motor neurons in *cdk-5(gm336)* and *cdk-5(ok626)* mutant animals using quantitative fluorescence microscopy. Both *cdk-5(ok626)* and *cdk-5(gm336)* alleles are predicted null mutations (Juo et al., 2007). We first imaged INS-22::Venus fluorescence in a posterior region of the dorsal nerve cord where it is only expressed in DB axons (Fig. 1*A*) and quantified the density and fluorescence intensities of INS-22::Venus puncta using custom written software (see Materials and Methods)(Burbea et al., 2002). INS-22::Venus puncta fluorescence intensities were decreased by about 35 to 40% ($p < 0.001$) in the motor neuron axons of *cdk-5(ok626)* and *cdk-5(gm336)* mutant animals compared to wild-type controls (Fig. 2*A–B*). We also analyzed the distribution of INS-22::Venus in DB motor neuron axons of animals with loss-of-function mutations in CDK-5's activator, CDKA-1/p35. Similarly, we found that INS-22::Venus puncta fluorescence intensities decreased by about 33% ($p<0.001$) in *cdka-1*(*gm335*) loss-of-function mutants compared to wild-type controls (Fig. 2*A–B*). There was no significant change in the density of INS-22::Venus puncta in DB motor neuron axons of *cdk-5* or *cdka-1* mutant animals (Fig. 2*C*). These results suggest that the abundance of INS-22-containing DCVs in the axons of DB motor neurons is regulated by CDK-5 and its activator CDKA-1/p35.

To determine if the loss of INS-22::Venus fluorescence in the axon was caused by alterations in neuropeptide trafficking in *cdk-5* mutants, we examined DB motor neuron cell bodies and dendrites for INS-22::Venus accumulation. We found no change in the abundance of INS-22::Venus in DB motor neuron cell bodies of *cdk-5(gm336)* mutants compared to controls (INS-22::Venus fluorescence (Norm.)±SEM: WT: 1.00±0.04; *cdk-5*: 1.02±0.05, $p>0.05$)(Fig. 6*B-C*), however, in the dendrites we found a significant increase ($p<0.001$) in INS-22::Venus puncta density in *cdk-5(ok626)*, *cdk-5(gm336),* and *cdka-1(gm335)* mutants (Fig. 2*D,F*). Furthermore, analysis of a DCV membrane marker, GFP-tagged IDA-1/IA-2 (insulinoma-associated protein 2)(Cai et al., 2004; Edwards et al., 2009; Solimena et al., 1996; Zhou et al., 2007), in wild type and *cdk-5* mutants revealed similar defects in the polarized distribution of DCVs in DB motor neurons (Fig. 2*G-L*). These results indicate that CDK-5 and its activator CDKA-1/p35 regulate the polarized distribution of DCVs in DB motor neurons.

CDK-5 functions cell autonomously in motor neurons to regulate DCV polarity

To determine if CDK-5 functions in motor neurons to regulate the polarized distribution of DCVs, we performed cell-type-specific rescue experiments. We found that the changes in INS-22::Venus puncta fluorescence intensities and densities in DB axons and dendrites of *cdk-5* mutants can be rescued by expression of wild-type *cdk-5* cDNA under the control of a DA/DB motor neuron-specific promoter, *Punc-129 (cdk-5* rescue)(Fig. 2*A-F*)(Sieburth et al., 2005). Likewise, the increase in INS-22::Venus puncta fluorescence intensity and density in DB dendrites of *cdka-1* mutants can be rescued by expression of wild-type *cdka-1* cDNA under the control of the *unc-129* promoter (*cdka-1* rescue)(Fig. 2*D–F*). Furthermore, expression of wild-type *cdk-5* cDNA under the control of a cholinergic neuron-specific promoter, *Punc-17* (*cdk-5* wt rescue) also rescued the increased accumulation of INS-22::Venus in the dendrites of *cdk-5*(*gm336*) mutants, whereas a kinase-dead version of

cdk-5 (*cdk-5* k.d. rescue) did not rescue (Average dendritic puncta density (per 10 μm) ±SEM: Wild type: 1.47±0.11; *cdk-5(gm336)*: 3.41±0.24; *cdk-5* w.t. rescue: 1.19±0.19; p<0.001 vs *cdk-5, cdk-5* k.d. rescue: 2.93±0.24, p>0.05 vs *cdk-5*). Together, these data indicate that CDK-5 and CDKA-1/p35 function in cholinergic motor neurons to regulate DCV polarity in a kinase activity-dependent manner.

CDK-5 regulates the polarized distribution of DCVs in DA motor neurons

We next investigated whether CDK-5 regulates the polarized distribution of DCVs in DA class motor neurons. Because there is some overlap between DA and DB processes in the nerve cords, we maximized our DA signal by analyzing regions of the DNC and VNC where the vast majority of INS-22::Venus was in DA motor neuron axons and dendrites, respectively (see Figure 1 and Materials and Methods). Although there was no change in the abundance of DCVs in *cdk-5* mutant DA axons (Average axonal puncta density (per 10μm) ±SEM: Wild type:4.38±0.16; *cdk-5(gm336)*: 4.12±0.21, p>0.05; Average axonal puncta intensity (Norm.)±SEM: Wild type: 1.0±0.07; *cdk-5(gm336)*: 0.86±0.05, p>0.05), *cdk-5* mutant dendrites had an increase in INS-22::Venus puncta density and intensity (Average dendritic puncta density (per 10 μm)±SEM: Wild type: 2.50±0.25; *cdk-5(gm336)*: 3.44±0.21, p<0.001; Average axonal puncta intensity (Norm.)±SEM: Wild type: 1.0±0.05; *cdk-5(gm336)*: 2.31±0.17, p<0.001). The DCV distribution defects observed in *cdk-5* mutant DA dendrites were rescued by expression of *cdk-5* cDNA under control of the *unc-129* promoter (Average dendritic puncta density (per 10 μm)±SEM: Wild type: 2.79±0.24; *cdk-5(gm336)*:3.92±0.21; *cdk-5* w.t. rescue:2.60±0.34; p<0.01 vs *cdk-5*; Average dendritic puncta intensity (Norm.)±SEM: Wild type: 1.0±0.06; *cdk-5(gm336)*: 2.01±0.15; *cdk-5* w.t. rescue:1.40±0.16; p<0.001 vs *cdk-5*). These data show that mutations in *cdk-5* result in defects in the polarized distribution of INS-22::Venus-containing DCVs in both DB and DA motor neurons. Interestingly, this result is in contrast to what was found for SVs, where CDK-5 was required for polarized SV trafficking in DA but not DB motor neurons (Ou et al., 2010). We focused the rest of our study on DB motor neurons because: (1) we can cleanly measure DCV signal in DB axons and dendrites, (2) *cdk-5* mutants have a stronger DCV polarity defect in DB neurons, and (3) polarized trafficking has not been studied in detail in DB neurons.

CDK-5 does not affect axon/dendrite morphology or markers

The defect in the polarized distribution of DCVs observed in *cdk-5* mutants could be due to defects in axon outgrowth or presynaptic development. To test this possibility, we analyzed the number and morphology of motor neurons in wild type and *cdk-5* mutants. We found no change in the number of motor neurons expressing INS-22::Venus under the control of the *Punc-129* promoter (# cell bodies±SEM: Wild type: 10.2±0.2; *cdk-5(gm336)*: 9.9±0.2; p>0.05) or in the gross morphology of their axonal and dendritic processes (data not shown). In addition, since the density of INS-22::Venus puncta in the axons of these motor neurons is unchanged in *cdk-5* and *cdka-1* mutant animals compared to controls (Fig. 2*C*), the number of presynaptic sites is likely unaltered. To further test for changes in presynaptic development, we examined the axonal distribution of the presynaptic active zone protein UNC-10/RIM-1. Fluorescently-tagged UNC-10 (under the control of the *Punc-129* promoter) localizes to synapses in the axons of DB motor neurons and is largely absent from the dendrites (Fig. 3*A,D*) (Sieburth et al., 2005). We found no significant change in UNC-10::GFP puncta fluorescence intensity (Fig. 3*B*) or density (Fig. 3C) in DB motor neuron axons of *cdk-5(gm336)* mutants compared to wild-type controls. We also examined the distribution of the synaptic vesicle (SV) marker GFP::RAB-3 in *cdk-5* mutants. GFP::RAB-3 localizes to synaptic sites in axons but not dendrites of wild type DB motor neurons (Fig. 3*E,H*)(Sieburth 2005), and this polarized distribution of SVs was unaltered in *cdk-5* mutants (Fig. 3*E,H*). We found no change in GFP::RAB-3 puncta density (Fig. 3*G*)

and no decrease in GFP::RAB-3 puncta intensity (Fig. 3*F*) in *cdk-5* mutant DB axons, and no increase in GFP::RAB-3 puncta in *cdk-5* mutant DB dendrites (Fig. 3*H*) compared to controls. These data are consistent with a recent study showing that *cdk-5* mutants do not have decreased SVs at presynaptic sites in DB motor neurons (Ou et al., 2010). These results suggest that the defect in the polarized distribution of DCVs observed in *cdk-5* mutants is not due to gross defects in axonal development. Thus, CDK-5 is required for the polarized distribution of DCVs, but not SVs, in DB motor neurons.

The increased abundance of DCVs in motor neuron dendrites could be the result of a general defect in dendritic trafficking that could, for example, be caused by a loss of dendrite identity. We tested this possibility by analyzing the distribution of two markers that have been shown to localize to the somatodendritic domain of DB motor neurons, Fibrillin FBN-1::GFP and the invertebrate GAP junction innexin protein UNC-9::GFP (Poon et al., 2008; Sieburth et al., 2005). We found normal somatodendritic localization of both UNC-9::GFP and FBN-1::GFP in *cdk-5* mutant animals, suggesting that a general defect in trafficking of dendritic proteins is unlikely (Fig. 3*I–L*). Together, these data indicate that the DCV localization defect observed in *cdk-5* mutants is not likely due to general defects in axon or dendrite development or the establishment and maintenance of axonal-dendritic polarity.

The effect of CDK-5 on DCV polarity is not likely a secondary consequence of synaptic transmission defects

CDK-5 can regulate synaptic transmission in other systems (Cheung et al., 2006; Dhavan and Tsai, 2001), and neuronal activity can regulate DCV trafficking (Shakiryanova et al., 2006). Thus, we tested whether the defect in the polarized distribution of DCVs in *cdk-5* mutants was a secondary consequence of a role for CDK-5 in synaptic transmission. In *C. elegans*, we found that *cdk-5* mutants have defects in synaptic transmission at the neuromuscular junction based on a behavioral paralysis assay using the acetylcholine esterase inhibitor aldicarb (Miller et al., 1996; Nguyen et al., 1995). Specifically, we found that *cdk-5* mutants have reduced sensitivity to aldicarb compared to wild-type animals (Animals paralyzed on aldicarb at 180 min (Percent±SEM): WT: 98±1.6%; *cdk-5(gm336)*: 45±0.74%), suggesting that *cdk-5* mutants have reduced synaptic transmission at the neuromuscular junction. If the changes in DCV polarity observed in *cdk-5* mutants were a secondary consequence of reduced synaptic transmission, then we would expect other synaptic transmission mutants to have similar defects in DCV polarity. Therefore, we analyzed whether INS-22::Venus-containing DCVs accumulate in motor neuron dendrites of *unc-10(e102)* mutants. UNC-10/RIM-1 is a RAB-3 interacting protein involved in synaptic vesicle priming, and loss-of-function mutations in *unc-10(e102)* mutants have stronger defects in synaptic transmission than *cdk-5* mutants based on the aldicarb-paralysis assay (Animals paralyzed on aldicarb at 180 min (Percent±SEM): WT: 98±1.6%, *cdk-5(gm336)*: 45±0.74%, *unc-10(e102)*: 3.3±3.3%)(Koushika et al., 2001; Miller et al., 1996; Nguyen et al., 1995). We found that, in contrast to our results in *cdk-5* mutants, there was no difference in the distribution of INS-22::Venus fluorescence in motor neuron dendrites of *unc-10* mutants (Dendritic puncta intensity (Norm.) ± SEM: WT: 1.0±0.06; *unc-10*: 0.87±0.07; $p>0.05$; Dendritic puncta density (per 10 μm)±SEM: WT: 1.74±0.16; *unc-10*: 1.85±0.22; $p>0.05$). This result indicates that the defect in the polarized distribution of DCVs observed in *cdk-5* mutant animals is not likely an indirect consequence of decreased synaptic transmission.

CDK-5 regulates microtubule polarity in motor neuron dendrites

Because the cytoskeleton plays a fundamental role in neuronal polarity and trafficking, we investigated whether CDK-5 affects microtubule orientation in DB motor neurons. In

mammals, microtubules in the axon are oriented plus-end out from the cell body, whereas microtubules in the dendrite are of mixed polarity (Baas et al., 1988; Burton, 1988; Stepanova et al., 2003). In *Drosophila* motor neurons and *C. elegans* amphid sensory neurons, while microtubules in the axon are also oriented plus-end out, the majority of microtubules in dendrites are minus-end out (Maniar et al., 2011; Rolls et al., 2007; Stone et al., 2008). We used microtubule plus-end binding protein dynamics to determine the orientation of microtubules in axons and dendrites of DB motor neurons (Mimori-Kiyosue et al., 2000; Stepanova et al., 2003; Stone et al., 2008). We used time-lapse microscopy and kymographs to analyze the movements of GFP-tagged EBP-1 (EBP-1::GFP), a *C. elegans* homolog of the microtubule plus-end binding protein EB1, in axons and dendrites of wild type and *cdk-5* mutants (see Materials and Methods). EBP-1::GFP puncta migrated at a velocity of 0.21±0.01 μm/s, consistent with reports of EB1 motion in other systems (Mimori-Kiyosue et al., 2000; Morrison et al., 2002). In wild type DB axons, we found that microtubule orientation was predominantly (96%) plus-end out from the cell body (Fig. 4*A,B*), which is consistent with previous reports of axonal microtubule orientation in *C. elegans*, *Drosophila,* and mammals (Baas et al., 1988; Maniar et al., 2011; Rolls et al., 2007; Stepanova et al., 2003; Stone et al., 2008). In wild type DB dendrites, we found that the majority of microtubules (91%) were oriented minus-end out from the cell body (Fig. 4*C,D*), which is similar to the dendritic microtubule orientation found in *Drosophila* motor neurons and *C. elegans* amphid sensory neurons (Maniar et al., 2011; Rolls et al., 2007; Stone et al., 2008). In *cdk-5* mutant axons, we found no change in the plus-end out microtubule orientation compared to wild type axons (Fig. 4*A,B*). However, in *cdk-5* mutant dendrites, we found a significant increase ($p<0.001$) in the percentage of plus-end out microtubules compared to wild type dendrites (Fig. 4*C,D*). These results indicate that CDK-5 regulates microtubule polarity in DB motor neuron dendrites.

CDK-5 regulates DCV trafficking in axons and dendrites

Because changes in microtubule polarity could lead to changes in DCV trafficking and ultimately DCV polarity, we next investigated whether CDK-5 regulates the trafficking of DCVs in DB motor neurons. DCVs are highly mobile and move bi-directionally in a saltatory fashion in both axons and dendrites of *C. elegans*, *Drosophila* and mammalian neurons (Barkus et al., 2008; de Jong et al., 2008; Gauthier et al., 2004; Kwinter et al., 2009; Zahn et al., 2004). Similarly, we observed a large fraction of INS-22::Venus puncta moving bi-directionally along motor neuron axons and dendrites (Fig. 5). To gain insight into why the polarized distribution of DCVs is disrupted in *cdk-5* mutant motor neurons, we performed time-lapse microscopy and kymograph analysis of mobile INS-22::Venus-containing vesicles in DB axon commissures and dendrites of wild-type and *cdk-5* mutant young adult animals (see Materials and Methods). We used these kymographs to calculate the velocity of mobile DCVs and to quantitate the number of DCVs moving away (anterograde) or towards (retrograde) the cell body. Although we were unable to calculate accurate velocities of DCVs in the axon commissure due to its curved trajectory, we found that in wild type dendrites, the average anterograde and retrograde DCV velocities were 1.29±0.07 μm/s and 0.97±0.05 μm/s, respectively, which is in agreement with previous reports of DCV velocities in *C. elegans* and mammals (Kwinter et al., 2009; Zahn et al., 2004).

Kymograph analysis of INS-22::Venus-containing DCVs in DB axon commissures revealed a decrease in the number of DCVs moving in the anterograde direction ($p<0.05$) and an increase in the number of stationary DCVs ($p<0.001$) in *cdk-5* mutants compared to controls (Fig. 5*A,B*). This trafficking defect correlates with a significant change ($p<0.001$) in the relative proportions of anterograde, retrograde and stationary DCVs in *cdk-5* mutants compared to controls (Fig. 5*C*), with no change in the total number of DCVs in the axon

commissure (Average number of total DCVs/kymograph±SEM: WT (n=23): 9.65±0.9, *cdk-5(gm336)*(n=25): 9.40±0.9, p>0.05). These data, taken together with the decrease in INS-22::Venus fluorescence at presynaptic sites in *cdk-5* mutant axons (Fig. 2*A,B*), are consistent with the idea that CDK-5 promotes anterograde DCV trafficking in DB axon commissures.

We also observed changes in DCV trafficking in DB dendrites of *cdk-5* mutants compared to wild-type controls (Fig. 5*D–F*). We discovered an increase in the total number of DCVs in dendrites of *cdk-5* mutants (Average number of total DCVs/kymograph±SEM: WT (n=34): 7.35±1.00; *cdk-5*(n=36): 12.47±1.23, p<0.01). Consistent with this, we found an increase in the number of stationary DCVs (p≤0.01), and an increase in the number of DCVs moving in both anterograde (p<0.05) and retrograde (p<0.05) directions in *cdk-5* mutant dendrites (Fig. 5*E*). However, there was no significant change (p>0.05) in the relative proportions of anterograde, retrograde and stationary DCVs in *cdk-5* mutant dendrites (Fig. 5*F*). Histogram analysis of the distribution of DCV velocities revealed an increase in the number of anterograde DCVs moving at a velocity of about 1–1.5 μm/s (Fig. 5*G*), although there was no change in the average anterograde and retrograde DCV velocities in *cdk-5* mutants (Average anterograde DCV velocity ± SEM(μm/s): WT: 1.29±0.07; *cdk-5*: 1.42±0.06, p>0.05, KS test; Average retrograde DCV velocity ± SEM(μm/s): WT: 0.97±0.05; *cdk-5*: 1.08±0.04, p>0.05, KS test). These results imply that in both wild type and *cdk-5* mutant dendrites, DCVs are transported on a motor that travels at 1–1.5 μm/s, but in *cdk-5* mutants there are more DCV trafficking events on this motor. Together, these data suggest that *cdk-5* mutants have increased DCVs in DB dendrites due to an increase in trafficking of DCVs into dendrites (i.e. anterograde trafficking), an increase in DCV accumulation (i.e. stationary DCVs) and a compensatory increase in retrograde DCV trafficking. Our time-lapse data, together with the increase in INS-22::Venus fluorescence in *cdk-5* mutant dendrites (Fig. 2*D,F*), are consistent with the idea that CDK-5 prevents trafficking of DCVs into DB dendrites.

We also used kymographs of INS-22::Venus movement to test whether *cdk-5* mutants have defects in the packaging of neuropeptides into DCVs in addition to their defects in DCV trafficking. Our steady-state imaging data show that INS-22::Venus puncta fluorescence intensity changes in *cdk-5* mutants (Fig. 2 and numbers reported in the text). Because each DCV contains many molecules of INS-22::Venus, changes in fluorescence intensity could represent either changes in the number of DCVs in each cluster (i.e. puncta) or changes in the amount of INS-22::Venus neuropeptides contained in each DCV. To distinguish between these possibilities, we measured the fluorescence intensity of mobile versus stationary INS-22::Venus puncta. Assuming that mobile puncta likely represent single DCVs, this analysis allows us to estimate the amount of INS-22::Venus neuropeptide contained in each DCV in wild type and *cdk-5* mutants. Histogram analysis of INS-22::Venus puncta fluorescence of mobile versus stationary puncta in wild type and *cdk-5* mutants supports the idea that *cdk-5* mutants have changes in the number of DCVs in each cluster (Fig. 5*H*). First, the average INS-22::Venus fluorescence intensity of mobile puncta was not altered in *cdk-5* mutants compared to wild type controls (Average puncta intensity (Norm.)±SEM: Wild type: 1.0±0.02, *cdk-5*: 0.95±0.02, p>0.05)(Fig. 5*H*). Second, INS-22::Venus fluorescence intensities of stationary puncta in *cdk-5* mutants shifted to higher values, revealing multiple peaks with increased fluorescence intensities compared to the intensities of mobile puncta (Fig. 5*H*). Assuming that mobile puncta largely represent single DCVs (see Materials and methods), these data are consistent with the idea that changes in INS-22::Venus puncta fluorescence observed in *cdk-5* mutant axons and dendrites are not due to changes in INS-22::Venus packaging, but likely represent changes in the number of DCVs per cluster. Thus, our data suggest that CDK-5 regulates polarized trafficking of DCVs in motor neurons. Taken together, our time-lapse analysis of DCVs in axons and dendrites are

consistent with a model where CDK-5 regulates the polarized distribution of DCVs by both promoting DCV trafficking in axons and inhibiting DCV trafficking into dendrites.

Role of kinesin UNC-104/KIF1Ain DCV trafficking

The increase in anterograde DCV trafficking and plus-end out microtubules in *cdk-5* mutant dendrites raises the question of whether a plus-end directed axonal motor, such as UNC-104/KIF1A (Hall and Hedgecock, 1991), is responsible for trafficking DCVs into dendrites. The kinesin UNC-104/KIF1A is required for the transport of DCVs to axons in *C. elegans* and *Drosophila* and has been reported to localize to dendrites as well as axons (Barkus et al., 2008; Jacob and Kaplan, 2003; Pack-Chung et al., 2007; Shin et al., 2003; Sieburth et al., 2005; Zahn et al., 2004; Zhou et al., 2001). In addition, a recent study showed that in PVD sensory neurons in *C. elegans*, UNC-104 was responsible for mis-trafficking axonal cargo into dendrites of *unc-33*/CRMP mutant animals (Maniar et al., 2011). We tested whether the increase in dendritic DCVs observed in *cdk-5* mutants was dependent on UNC-104 by analyzing *cdk-5;unc-104* double mutant animals. Consistent with its role in axonal DCV transport, we found little to no INS-22::Venus fluorescence in motor neuron axons (Fig 6*A*) and a corresponding increase in the amount of INS-22::Venus in the cell bodies and dendrites of *unc-104(e1265)* loss-of-function mutants (Fig. 6*B–F*)(Sieburth et al., 2005). If UNC-104-dependent trafficking is responsible for the increased accumulation of DCVs in *cdk-5* mutant dendrites, then this increase should be blocked by *unc-104* mutations. In contrast, we found a significant increase in INS-22::Venus fluorescence intensity in *cdk-5;unc-104* double mutant dendrites compared to either single mutant or wild type controls (Fig. 6*E*). However, we did not observe a corresponding additive increase in INS-22::Venus puncta density in the double mutants (Fig. 6*F*). This data, together with our histogram analysis of INS-22::Venus content in DCVs (Fig. 5*H*), suggests that the number of DCV accumulation sites in *cdk-5;unc-104* double mutant dendrites may have reached its upper limit and that the further increase in intensity represents the addition of more DCVs to existing clusters. Thus, the increased abundance of INS-22::Venus fluorescence in *cdk-5;unc-104* double mutant dendrites suggests that kinesin UNC-104 is not required for the DCV accumulation in *cdk-5* mutant dendrites. Interestingly, the accumulation of DCVs in the cell bodies of *unc-104* mutants decreased in *unc-104;cdk-5* double mutants concomitantly with the increase in the dendrites (Fig. 6*B–C*). These results suggest that CDK-5 may function at the cell body to inhibit trafficking of DCVs into dendrites.

The increase in DCVs observed in *cdk-5* mutant dendrites requires cytoplasmic dynein

Because mutations in *unc-104* did not block the DCV polarity defect in *cdk-5* mutants and the majority (67%) of microtubules in *cdk-5* mutant dendrites are still oriented minus-end out from the cell body, we tested whether the major minus-end directed motor, cytoplasmic dynein, was responsible for trafficking DCVs into *cdk-5* mutant dendrites. Cytoplasmic dynein has been shown to traffic DCVs carrying BDNF and has recently been shown to traffic pre- and postsynaptic cargoes into dendrites (Colin et al., 2008; Gauthier et al., 2004; Kapitein et al., 2010; Ou et al., 2010). We found that loss of function mutations in the heavy chain of dynein, *dhc-1(js319)*(Koushika et al., 2004) or light-intermediate chain of dynein, *dli-1(ku266)*(Yoder and Han, 2001), completely block the increase in DCVs in *cdk-5* mutant dendrites (Fig. 7*D,F*, and data not shown). This result indicates that cytoplasmic dynein is required for the increase in DCVs observed in the dendrites of *cdk-5* mutants.

Our results show that CDK-5 regulates two aspects of neuronal polarity: polarized DCV trafficking and microtubule orientation. Because dynein motor function has been reported to be required for the uniform plus-end out microtubule orientation in *Drosophila* axons (Zheng et al., 2008), and microtubule organization in non-neuronal cells (Smith et al., 2000), we investigated whether the effects of CDK-5 on neuronal polarity were related.

Specifically, we tested whether *dynein* mutations suppress the change in microtubule orientation observed in *cdk-5* mutant dendrites by analyzing kymographs of EBP-1::GFP dynamics in DB axons and dendrites of *dhc-1* single and *cdk-5;dhc-1* double mutants. We found no significant changes in the plus-end out microtubule orientation in axons of *dhc-1* single or *dhc-1;cdk-5* double mutants (Fig. 7*G*). Similarly, we found no differences in the largely minus-end out microtubule orientation in dendrites of *dhc-1* mutants compared to wild type controls (Fig. 7*H*). Finally, there was no significant difference ($p>0.05$) between the increased proportion of plus-end out microtubules observed in *cdk-5* single and *cdk-5;dhc-1* double mutant dendrites (Fig. 7*H*). These results suggest that the *dhc-1(js319)* dynein mutation does not affect microtubule orientation in DB axons and dendrites. Thus, the ability of the *dhc-1(js319)* dynein mutation to suppress the accumulation of DCVs in *cdk-5* mutant dendrites cannot be attributed to potential effects of dynein on microtubule polarity, and our findings are more consistent with a model where CDK-5 inhibits dynein-dependent trafficking of DCVs into dendrites.

We next analyzed the role of dynein in DB axons of wild type and *cdk-5* mutant animals. We found a significant increase in INS-22::Venus puncta fluorescence intensity in *dhc-1* single mutant axons (Fig. 7*A,B*), consistent with a role for dynein in retrograde DCV trafficking in the axon. As described above, *cdk-5* single mutants have decreased abundance of DCVs in DB axons (Fig. 2*A,B* and 7*A,B*). If the decrease in axonal DCVs observed in *cdk-5* mutants was mediated by dynein, then this decrease should be blocked by mutations in dynein. However, we found that *dhc-1* mutation only partially suppressed the decrease in DCV accumulation observed in *cdk-5* mutant axons (Fig. 7*A,B*). This result suggests that in DB motor neuron axons CDK-5 and dynein may function in separate pathways to regulate DCV accumulation. This result is consistent with our time-lapse analysis showing that CDK-5 does not inhibit retrograde DCV trafficking in axons but rather promotes anterograde DCV trafficking (Fig. 5*B*). However, because the *dhc-1(js319)* allele is not a null mutation, we cannot exclude the possibility that the partial effect of *dhc-1* mutation on DCV trafficking in *cdk-5* mutant axons may be due to an incomplete loss of dynein function.

Dynein is required for increased trafficking of DCVs in *cdk-5* mutant dendrites

Our time-lapse analysis of DCV movement shows that *cdk-5* mutants have increased numbers of mobile (anterogradely and retrogradely moving DCVs) and stationary DCVs in dendrites (Fig. 5*E*). In order to investigate whether dynein regulates DCV trafficking in dendrites, we performed time-lapse analysis of mobile INS-22::Venus puncta in *dhc-1* single and *cdk-5;dhc-1* double mutants. We found a significant decrease in the number of DCVs moving in the anterograde and retrograde directions in *dhc-1* single mutant dendrites (Fig. 8*A*). These data indicate that dynein is required for DCV trafficking in the dendrites of wild-type animals. Furthermore, *dhc-1* mutation blocked the increase in anterograde and retrograde DCV trafficking (Fig. 8*A*) and total number of DCVs observed in *cdk-5* mutant dendrites (Number of DCVs/kymograph: WT:7.35±1.00; *cdk-5*: 12.47±1.23; *dhc-1*: 3.43±0.52; *cdk-5;dhc-1*: 5.96±1.2; *cdk-5;dhc-1* vs. *cdk-5,* $p<0.001$; *cdk-5;dhc-1* vs wt and *dhc-1*, $p>0.05$). These results are consistent with our steady-state imaging data in *cdk-5;dhc-1* double mutants (Fig. 7*D,F*) and suggest that dynein is required for anterograde DCV trafficking in dendrites. Although dynein may also participate in retrograde DCV trafficking, the decrease in the total number of DCVs in dendrites of *cdk-5;dhc-1* double mutants (Fig. 7*D,F*) suggest that changes in retrograde trafficking may be a secondary consequence of decreased anterograde DCV trafficking. Thus, our data suggest a model where CDK-5 inhibits anterograde trafficking of dynein in general, or more specifically, inhibits trafficking of dynein-DCV complexes into dendrites.

In order to test whether CDK-5 inhibits general trafficking of dynein into dendrites, we analyzed the distribution of a dynein associated protein, GFP-tagged dynein light-intermediate chain (DLI-1::GFP), in DB dendrites of wild type and *cdk-5* mutants. We found that the distribution of DLI-1::GFP was diffuse throughout most of the dendrite, but accumulated at the distal tips of DB dendrites, consistent with their predominantly minus-end out microtubule orientation and DLI-1 association with dynein. We found no change in the amount of DLI-1::GFP fluorescence at the distal dendrite tips in *cdk-5* mutants compared to wild type controls (Fig. 8*B–C*). Thus, CDK-5 may not regulate overall trafficking of dynein into dendrites, but may have a more specific effect on the trafficking of DCVs by dynein. Taken together, these results suggest that cytoplasmic dynein is required for the increased trafficking and accumulation of DCVs in *cdk-5* mutant dendrites, and are consistent with a model where CDK-5 inhibits loading of DCVs onto dynein or trafficking of dynein-DCV complexes into dendrites.

Discussion

CDK-5 regulates polarized trafficking of DCVs

We investigated the role of CDK-5 in neuronal polarity and found that CDK-5 and its activator CDKA-1/p35 are required for the polarized distribution of neuropeptide-containing DCVs in DA and DB cholinergic motor neurons (Fig. 2). Time-lapse microscopy of mobile DCVs in DB neurons revealed that *cdk-5* mutation results in decreased trafficking of DCVs into axons and increased trafficking and accumulation of DCVs because *cdk-5* mutants had no obvious defect in the polarized distribution of axonal markers, such as SVs, or dendritic markers (Fig. 3). There are several potential models to explain the mechanism by which CDK-5 regulates polarized DCV trafficking:

1. The axonal DCV motor UNC-104 mistraffics into dendrites in *cdk-5* mutants. In *unc-104* mutants, DCVs do not traffic properly to axons and accumulate in motor neuron cell bodies and dendrites (Fig. 6)(Sieburth et al., 2005). If this model were correct, then genetically removing *unc-104* in *cdk-5* mutants should not increase the DCV trafficking defect of *cdk-5* single mutants. Instead, we found that *cdk-5;unc-104* double mutants had an increased abundance of DCVs in dendrites compared to either single mutant (Fig. 6*D-F*). Thus, we think this model is unlikely.

2. DCVs are trafficked to both axons and dendrites and CDK-5 promotes retrograde trafficking of DCVs from dendrites back to the cell bodies. If this model were correct, then *cdk-5* mutants should have decreased numbers of retrogradely moving DCVs in dendrites. Our time-lapse analysis of mobile DCVs showed that *cdk-5* mutants do not have decreased retrograde DCV trafficking but instead have increased amounts of DCV trafficking in dendrites (Fig. 5*E*), suggesting that this model is also unlikely.

3. CDK-5 positively regulates axonal trafficking of DCVs on kinesin UNC-104. For example, CDK-5 might directly promote the loading of DCVs onto UNC-104 or promote anterograde trafficking of UNC-104 into axons. If this model were correct, then *cdk-5* mutants should have decreased anterograde DCV trafficking in the axon and *cdk-5;unc-104* double mutants should have a non-additive effect on DCVs in the dendrites. Consistent with this model, we found that *cdk-5* mutants have decreased anterograde DCV trafficking in axon commissures (Fig. 5*B*), however, we also found that *cdk-5;unc-104* double mutants have additive increases in DCVs in dendrites (Fig. 6*D–F*). Thus, CDK-5 appears to promote UNC-104-dependent anterograde trafficking of DCVs in axons, however our genetic data suggest that this cannot be the only mechanism by which CDK-5 regulates DCV polarity.

4. CDK-5 inhibits the transport of DCVs into dendrites. Our data are also consistent with this model. First, *cdk-5* mutants have increased amounts of DCVs trafficking into and accumulating in dendrites (Figs. 2 and 5). Second, the cell body accumulation of DCVs observed in *unc-104* single mutants is reduced to wild type levels in *cdk-5;unc-104* double mutants along with a concomitant increase of DCVs in dendrites (Fig. 6). Third, mutations in the minus-end-directed motor cytoplasmic dynein completely block the increased trafficking of DCVs in *cdk-5* mutant dendrites (Figs. 7 and 8).

In summary, our data support a model where CDK-5 regulates DCV polarity by both promoting axonal DCV trafficking and inhibiting dendritic DCV trafficking.

CDK-5 regulates microtubule polarity

This study also identifies CDK-5 as a novel regulator of microtubule polarity. We used the microtubule plus-end binding protein EBP-1 to describe the orientation of microtubules in cholinergic motor neurons and found that in wild type animals, DB axons have predominantly plus-end out microtubule polarity, whereas DB dendrites have a slightly less uniform orientation with the vast majority of microtubules being oriented with their minus-ends distal to the cell body (Fig. 4). These results are consistent with the microtubule polarity inferred from analysis of tailless motors in DA motor neurons (Ou et al., 2010), and of EB protein dynamics in amphid sensory neurons in *C. elegans* (Maniar et al., 2011) and *Drosophila* (Rolls et al., 2007; Stone et al., 2008; Zheng et al., 2008). Although *cdk-5* mutants do not affect microtubule orientation in DB motor neuron axons (Fig. 4*A,B*), we found, surprisingly, that *cdk-5* mutants have an increase in plus-end out microtubules in DB dendrites (Fig. 4*C,D*). While the precise molecular mechanism involved is not known, it will be interesting to test in future studies whether CDK-5's effect on microtubule polarity is mediated by it's ability to phosphorylate microtubule-associated proteins (Dhavan and Tsai, 2001; Hou et al., 2007; Kaminosono et al., 2008; Patrick et al., 1999; Tanaka et al., 2004; Wada et al., 1998).

Because CDK-5 affects the polarized trafficking of DCVs and microtubule orientation, we tested whether these two polarity effects were related. Our data suggest that CDK-5's effect on microtubule polarity cannot explain the increased trafficking of DCVs into dendrites. Dynein mutations completely block the increased trafficking and accumulation of DCVs in *cdk-5* mutant dendrites (Fig. 7 and 8) without affecting the *cdk-5*-dependent change in microtubule polarity (Fig. 7*H*). Interestingly, the normal polarized distribution of several axonal and dendritic markers (Fig. 3) and the normal accumulation of the dynein complex protein DLI-1::GFP at the distal tips of dendrites in *cdk-5* mutants (Fig. 8*B,C*), suggest that these mutants do not have gross defects in polarized transport. Thus, robust and redundant cellular mechanisms may exist to establish and maintain neuronal polarity. Alternatively, the magnitude of CDK-5's effect on microtubule polarity may not be large enough to result in obvious polarity defects, or the effect of *cdk-5* on microtubule orientation may result in defects in the polarized trafficking of other cargo or aspects of neuronal polarity that we did not examine.

Comparison of SV and DCV trafficking by CDK-5

SVs are also trafficked in a polarized manner to presynaptic sites in axons and many genes and mechanisms involved in this trafficking have been described in cultured hippocampal neurons (West et al., 1997) and *C. elegans* motor neurons (Byrd et al., 2001; Crump et al., 2001; Hung et al., 2007; Ou et al., 2010; Ou and Shen, 2010; Poon et al., 2008; Sakaguchi-Nakashima et al., 2007; Sakamoto et al., 2005; Tanizawa et al., 2006). A recent study showed that CDK-5 regulates the polarized trafficking of SV precursors to axons by inhibiting cytoplasmic dynein (Ou et al., 2010). Similarly, we found that polarized DCV

trafficking is also dependent on CDK-5 and dynein. Thus, despite the differences between SVs and DCVs, CDK-5 can promote the polarized trafficking of both vesicle types. There are several interesting differences between CDK-5 regulation of SV and DCV polarity. First, Ou et al (2010) found that CDK-5 was required for polarized trafficking of SVs in DA class motor neurons but, surprisingly, not in DB class motor neurons (Ou et al., 2010). In contrast, we found that the polarized distribution of DCVs requires *cdk-5* in both DA and DB motor neurons. The precise reason for this difference is not clear. However, these studies suggest that SV polarity is regulated by multiple and redundant mechanisms that differ between DA and DB neurons, whereas DCV polarity requires CDK-5 activity in both cell types. Second, Ou et al. (2010) used time-lapse analysis of SVs in DA axons to show that CDK-5 inhibits trafficking of SVs back to the cell body in a dynein-dependent manner (Ou et al., 2010). In contrast, we found that CDK-5 functions to promote DCV trafficking in DB axons, suggesting that CDK-5 may promote loading of DCVs onto UNC-104 or trafficking of UNC-104-DCV complexes into axons. While positive regulation of UNC-104 by CDK-5 does not appear to be relevant for SV polarity in DA axons, CDK-5 can promote UNC-104-dependent trafficking in axons of GABAergic DD motor neurons (Park et al., 2011). In addition to promoting axonal DCV trafficking, we show that CDK-5 also prevents trafficking of DCVs into DB dendrites in a dynein-dependent manner. This data is consistent with the idea that CDK-5 may prevent the trafficking of DCVs into dendrites either by inhibiting the loading of DCVs onto dynein or by inhibiting trafficking of dynein-DCV complexes into dendrites. One simple model that may explain these two effects of CDK-5 on DCV trafficking in DB axons and dendrites would be as follows: CDK-5 phosphorylates a protein (e.g. a specific DCV adaptor), which then promotes association of DCVs with UNC-104 in the cell body and also inhibits association with dynein. In this manner, CDK-5 phosphorylation of this DCV-specific protein would act as a switch to both promote trafficking of DCVs into axons and inhibit trafficking of DCVs into dendrites. By analogy, CDK-5 might phosphorylate a SV-specific protein to differentially regulate its polarized trafficking. Further experiments will be necessary to identify the relevant SV-and DCV-specific proteins to test this model.

In closing, while CDK-5 can regulate the polarized trafficking of SV precursors and DCVs destined for axons, the dependence on CDK-5 and the precise trafficking mechanisms involved appear to differ between neuronal cell types and vesicular cargos. Because DCVs are diverse and can transport cargo destined for secretion in dendrites, much remains to be learned about the molecular mechanisms involved in trafficking of different DCV populations to specific destinations.

Acknowledgments

We would like to thank Josh Kaplan, Lars Dreier, QueeLim Ch'ng, Derek Sieburth and Jeremy Dittman for advice, reagents and comments on this manuscript. We thank Michele Jacob, Victor Hatini, Jennifer Kowalski and members of the Juo lab for helpful discussions and comments on this manuscript, and Jeremy Dittman and Dan Cox for data analysis software. We would also like to thank Kang Shen for generously sharing unpublished data and Gian Garriga, Ken Miller, Naoki Hisamoto, the CGC and Shohei Mitani for plasmids and strains. This research was supported by a grant from the National Institutes of Health (NIH) to P.J. (NS059953), a Basil O'Connor March of Dimes Scholar Award to P.J. and the Tufts Center for Neuroscience Research (P30 NS047243). PRG was supported by a Dean's Fellowship and the Synapse Neurobiology Training Program (T32 NS061764).

References

Baas PW, Deitch JS, Black MM, Banker GA. Polarity orientation of microtubules in hippocampal neurons: uniformity in the axon and nonuniformity in the dendrite. Proc Natl Acad Sci U S A. 1988; 85:8335–9. [PubMed: 3054884]

Barkus RV, Klyachko O, Horiuchi D, Dickson BJ, Saxton WM. Identification of an axonal kinesin-3 motor for fast anterograde vesicle transport that facilitates retrograde transport of neuropeptides. Mol Biol Cell. 2008; 19:274–83. [PubMed: 17989365]

Borgonovo B, Ouwendijk J, Solimena M. Biogenesis of secretory granules. Curr Opin Cell Biol. 2006; 18:365–70. [PubMed: 16806882]

Burbea M, Dreier L, Dittman JS, Grunwald ME, Kaplan JM. Ubiquitin and AP180 regulate the abundance of GLR-1 glutamate receptors at postsynaptic elements in *C. elegans*. Neuron. 2002; 35:107–20. [PubMed: 12123612]

Burton PR. Dendrites of mitral cell neurons contain microtubules of opposite polarity. Brain Res. 1988; 473:107–15. [PubMed: 3264743]

Byrd DT, Kawasaki M, Walcoff M, Hisamoto N, Matsumoto K, Jin Y. UNC-16, a JNK-signaling scaffold protein, regulates vesicle transport in *C. elegans*. Neuron. 2001; 32:787–800. [PubMed: 11738026]

Cai T, Fukushige T, Notkins AL, Krause M. Insulinoma-Associated Protein IA-2, a Vesicle Transmembrane Protein, Genetically Interacts with UNC-31/CAPS and Affects Neurosecretion in *Caenorhabditis elegans*. J Neurosci. 2004; 24:3115–24. [PubMed: 15044551]

Ch'ng Q, Sieburth D, Kaplan JM. Profiling synaptic proteins identifies regulators of insulin secretion and lifespan. PLoS Genet. 2008; 4:e1000283. [PubMed: 19043554]

Chalfie M, Sulston JE, White JG, Southgate E, Thomson JN, Brenner S. The neural circuit for touch sensitivity in *Caenorhabditis elegans*. J Neurosci. 1985; 5:956–64. [PubMed: 3981252]

Cheung ZH, Fu AK, Ip NY. Synaptic roles of Cdk5: implications in higher cognitive functions and neurodegenerative diseases. Neuron. 2006; 50:13–8. [PubMed: 16600851]

Colin E, Zala D, Liot G, Rangone H, Borrell-Pages M, Li XJ, Saudou F, Humbert S. Huntingtin phosphorylation acts as a molecular switch for anterograde/retrograde transport in neurons. Embo J. 2008; 27:2124–34. [PubMed: 18615096]

Crump JG, Zhen M, Jin Y, Bargmann CI. The SAD-1 kinase regulates presynaptic vesicle clustering and axon termination. Neuron. 2001; 29:115–29. [PubMed: 11182085]

de Jong EK, Vinet J, Stanulovic VS, Meijer M, Wesseling E, Sjollema K, Boddeke HW, Biber K. Expression, transport, and axonal sorting of neuronal CCL21 in large dense-core vesicles. Faseb J. 2008; 22:4136–45. [PubMed: 18697841]

Dhavan R, Tsai LH. A decade of CDK5. Nat Rev Mol Cell Biol. 2001; 2:749–59. [PubMed: 11584302]

Dikeakos JD, Reudelhuber TL. Sending proteins to dense core secretory granules: still a lot to sort out. J Cell Biol. 2007; 177:191–6. [PubMed: 17438078]

Edwards SL, Charlie NK, Richmond JE, Hegermann J, Eimer S, Miller KG. Impaired dense core vesicle maturation in *Caenorhabditis elegans* mutants lacking Rab2. J Cell Biol. 2009; 186:881–95. [PubMed: 19797080]

Fisher JM, Sossin W, Newcomb R, Scheller RH. Multiple neuropeptides derived from a common precursor are differentially packaged and transported. Cell. 1988; 54:813–22. [PubMed: 3409320]

Gauthier LR, Charrin BC, Borrell-Pages M, Dompierre JP, Rangone H, Cordelieres FP, De Mey J, MacDonald ME, Lessmann V, Humbert S, Saudou F. Huntingtin controls neurotrophic support and survival of neurons by enhancing BDNF vesicular transport along microtubules. Cell. 2004; 118:127–38. [PubMed: 15242649]

Hall DH, Hedgecock EM. Kinesin-related gene unc-104 is required for axonal transport of synaptic vesicles in *C. elegans*. Cell. 1991; 65:837–47. [PubMed: 1710172]

Hammarlund M, Watanabe S, Schuske K, Jorgensen EM. CAPS and syntaxin dock dense core vesicles to the plasma membrane in neurons. J Cell Biol. 2008; 180:483–91. [PubMed: 18250196]

Haspel G, O'Donovan MJ, Hart AC. Motoneurons dedicated to either forward or backward locomotion in the nematode *Caenorhabditis elegans*. J Neurosci. 2010; 30:11151–6. [PubMed: 20720122]

Horton AC, Ehlers MD. Neuronal polarity and trafficking. Neuron. 2003; 40:277–95. [PubMed: 14556709]

Hou Z, Li Q, He L, Lim HY, Fu X, Cheung NS, Qi DX, Qi RZ. Microtubule association of the neuronal p35 activator of Cdk5. J Biol Chem. 2007; 282:18666–70. [PubMed: 17491008]

Hung W, Hwang C, Po MD, Zhen M. Neuronal polarity is regulated by a direct interaction between a scaffolding protein, Neurabin, and a presynaptic SAD-1 kinase in *Caenorhabditis elegans*. Development. 2007; 134:237–49. [PubMed: 17151015]

Jacob TC, Kaplan JM. The EGL-21 carboxypeptidase E facilitates acetylcholine release at *Caenorhabditis elegans* neuromuscular junctions. J Neurosci. 2003; 23:2122–30. [PubMed: 12657671]

Juo P, Harbaugh T, Garriga G, Kaplan JM. CDK-5 regulates the abundance of GLR-1 glutamate receptors in the ventral cord of *Caenorhabditis elegans*. Mol Biol Cell. 2007; 18:3883–93. [PubMed: 17671168]

Kaminosono S, Saito T, Oyama F, Ohshima T, Asada A, Nagai Y, Nukina N, Hisanaga S. Suppression of mutant Huntingtin aggregate formation by Cdk5/p35 through the effect on microtubule stability. J Neurosci. 2008; 28:8747–55. [PubMed: 18753376]

Kapitein LC, Schlager MA, Kuijpers M, Wulf PS, van Spronsen M, MacKintosh FC, Hoogenraad CC. Mixed microtubules steer dynein-driven cargo transport into dendrites. Curr Biol. 2010; 20:290–9. [PubMed: 20137950]

Koushika SP, Richmond JE, Hadwiger G, Weimer RM, Jorgensen EM, Nonet ML. A post-docking role for active zone protein Rim. Nat Neurosci. 2001; 4:997–1005. [PubMed: 11559854]

Koushika SP, Schaefer AM, Vincent R, Willis JH, Bowerman B, Nonet ML. Mutations in *Caenorhabditis elegans* cytoplasmic dynein components reveal specificity of neuronal retrograde cargo. J Neurosci. 2004; 24:3907–16. [PubMed: 15102906]

Kwinter DM, Lo K, Mafi P, Silverman MA. Dynactin regulates bidirectional transport of dense-core vesicles in the axon and dendrites of cultured hippocampal neurons. Neuroscience. 2009; 162:1001–10. [PubMed: 19497353]

Landry M, Vila-Porcile E, Hokfelt T, Calas A. Differential routing of coexisting neuropeptides in vasopressin neurons. Eur J Neurosci. 2003; 17:579–89.

Lessmann V, Brigadski T. Mechanisms, locations, and kinetics of synaptic BDNF secretion: an update. Neurosci Res. 2009; 65:11–22. [PubMed: 19523993]

Li, C.; Kim, K. Neuropeptides. WormBook; 2008. p. 1-36.

Maniar TA, Kaplan M, Wang GJ, Shen K, Wei L, Shaw JE, Koushika SP, Bargmann CI. UNC-33 (CRMP) and ankyrin organize microtubules and localize kinesin to polarize axon-dendrite sorting. Nat Neurosci. 2011; 15:48–56. [PubMed: 22101643]

Miller KG, Alfonso A, Nguyen M, Crowell JA, Johnson CD, Rand JB. A genetic selection for *Caenorhabditis elegans* synaptic transmission mutants. Proc Natl Acad Sci U S A. 1996; 93:12593–8. [PubMed: 8901627]

Mimori-Kiyosue Y, Shiina N, Tsukita S. The dynamic behavior of the APC-binding protein EB1 on the distal ends of microtubules. Curr Biol. 2000; 10:865–8. [PubMed: 10899006]

Morfini G, Szebenyi G, Brown H, Pant HC, Pigino G, DeBoer S, Beffert U, Brady ST. A novel CDK5-dependent pathway for regulating GSK3 activity and kinesin-driven motility in neurons. Embo J. 2004; 23:2235–45. [PubMed: 15152189]

Morrison EE, Moncur PM, Askham JM. EB1 identifies sites of microtubule polymerisation during neurite development. Brain Res Mol Brain Res. 2002; 98:145–52. [PubMed: 11834307]

Nguyen M, Alfonso A, Johnson CD, Rand JB. *Caenorhabditis elegans* mutants resistant to inhibitors of acetylcholinesterase. Genetics. 1995; 140:527–35. [PubMed: 7498734]

Ou CY, Poon VY, Maeder CI, Watanabe S, Lehrman EK, Fu AK, Park M, Fu WY, Jorgensen EM, Ip NY, Shen K. Two cyclin-dependent kinase pathways are essential for polarized trafficking of presynaptic components. Cell. 2010; 141:846–58. [PubMed: 20510931]

Ou CY, Shen K. Neuronal polarity in *C. elegans*. Dev Neurobiol. 2010; 71:554–66. [PubMed: 21557505]

Pack-Chung E, Kurshan PT, Dickman DK, Schwarz TL. A Drosophila kinesin required for synaptic bouton formation and synaptic vesicle transport. Nat Neurosci. 2007; 10:980–9. [PubMed: 17643120]

Pandey JP, Smith DS. A cdk5-dependent switch regulates lis1/ndel1/dynein-driven organelle transport in adult axons. J Neurosci. 2011; 31:17207–19. [PubMed: 22114287]

Park M, Watanabe S, Poon VY, Ou CY, Jorgensen EM, Shen K. CYY-1/cyclin Y and CDK-5 differentially regulate synapse elimination and formation for rewiring neural circuits. Neuron. 2011; 70:742–57. [PubMed: 21609829]

Patrick GN, Zukerberg L, Nikolic M, de la Monte S, Dikkes P, Tsai LH. Conversion of p35 to p25 deregulates Cdk5 activity and promotes neurodegeneration. Nature. 1999; 402:615–22. [PubMed: 10604467]

Pierce SB, Costa M, Wisotzkey R, Devadhar S, Homburger SA, Buchman AR, Ferguson KC, Heller J, Platt DM, Pasquinelli AA, Liu LX, Doberstein SK, Ruvkun G. Regulation of DAF-2 receptor signaling by human insulin and ins-1, a member of the unusually large and diverse *C. elegans* insulin gene family. Genes Dev. 2001; 15:672–86. [PubMed: 11274053]

Poon VY, Klassen MP, Shen K. UNC-6/netrin and its receptor UNC-5 locally exclude presynaptic components from dendrites. Nature. 2008; 455:669–73. [PubMed: 18776887]

Ratner N, Bloom GS, Brady ST. A role for cyclin-dependent kinase(s) in the modulation of fast anterograde axonal transport: effects defined by olomoucine and the APC tumor suppressor protein. J Neurosci. 1998; 18:7717–26. [PubMed: 9742142]

Rolls MM, Satoh D, Clyne PJ, Henner AL, Uemura T, Doe CQ. Polarity and intracellular compartmentalization of *Drosophila* neurons. Neural Dev. 2007; 2:7. [PubMed: 17470283]

Sakaguchi-Nakashima A, Meir JY, Jin Y, Matsumoto K, Hisamoto N. LRK-1, a *C. elegans* PARK8-related kinase, regulates axonal-dendritic polarity of SV proteins. Curr Biol. 2007; 17:592–8. [PubMed: 17346966]

Sakamoto R, Byrd DT, Brown HM, Hisamoto N, Matsumoto K, Jin Y. The *Caenorhabditis elegans* UNC-14 RUN domain protein binds to the kinesin-1 and UNC-16 complex and regulates synaptic vesicle localization. Mol Biol Cell. 2005; 16:483–96. [PubMed: 15563606]

Shakiryanova D, Tully A, Levitan ES. Activity-dependent synaptic capture of transiting peptidergic vesicles. Nat Neurosci. 2006; 9:896–900. [PubMed: 16767091]

Shin H, Wyszynski M, Huh KH, Valtschanoff JG, Lee JR, Ko J, Streuli M, Weinberg RJ, Sheng M, Kim E. Association of the kinesin motor KIF1A with the multimodular protein liprin-alpha. J Biol Chem. 2003; 278:11393–401. [PubMed: 12522103]

Sieburth D, Ch'ng Q, Dybbs M, Tavazoie M, Kennedy S, Wang D, Dupuy D, Rual JF, Hill DE, Vidal M, Ruvkun G, Kaplan JM. Systematic analysis of genes required for synapse structure and function. Nature. 2005; 436:510–7. [PubMed: 16049479]

Sieburth D, Madison JM, Kaplan JM. PKC-1 regulates secretion of neuropeptides. Nat Neurosci. 2007; 10:49–57. [PubMed: 17128266]

Smith DS, Niethammer M, Ayala R, Zhou Y, Gambello MJ, Wynshaw-Boris A, Tsai LH. Regulation of cytoplasmic dynein behaviour and microtubule organization by mammalian Lis1. Nat Cell Biol. 2000; 2:767–75. [PubMed: 11056530]

Solimena M, Dirkx R Jr, Hermel JM, Pleasic-Williams S, Shapiro JA, Caron L, Rabin DU. ICA 512, an autoantigen of type I diabetes, is an intrinsic membrane protein of neurosecretory granules. Embo J. 1996; 15:2102–14. [PubMed: 8641276]

Stepanova T, Slemmer J, Hoogenraad CC, Lansbergen G, Dortland B, De Zeeuw CI, Grosveld F, van Cappellen G, Akhmanova A, Galjart N. Visualization of microtubule growth in cultured neurons via the use of EB3-GFP (end-binding protein 3-green fluorescent protein). J Neurosci. 2003; 23:2655–64. [PubMed: 12684451]

Stone MC, Roegiers F, Rolls MM. Microtubules have opposite orientation in axons and dendrites of *Drosophila* neurons. Mol Biol Cell. 2008; 19:4122–9. [PubMed: 18667536]

Sumakovic M, Hegermann J, Luo L, Husson SJ, Schwarze K, Olendrowitz C, Schoofs L, Richmond J, Eimer S. UNC-108/RAB-2 and its effector RIC-19 are involved in dense core vesicle maturation in *Caenorhabditis elegans*. J Cell Biol. 2009; 186:897–914. [PubMed: 19797081]

Tanaka T, Serneo FF, Tseng HC, Kulkarni AB, Tsai LH, Gleeson JG. Cdk5 phosphorylation of doublecortin ser297 regulates its effect on neuronal migration. Neuron. 2004; 41:215–27. [PubMed: 14741103]

Tanizawa Y, Kuhara A, Inada H, Kodama E, Mizuno T, Mori I. Inositol monophosphatase regulates localization of synaptic components and behavior in the mature nervous system of *C. elegans*. Genes Dev. 2006; 20:3296–310. [PubMed: 17158747]

Wada Y, Ishiguro K, Itoh TJ, Uchida T, Hotani H, Saito T, Kishimoto T, Hisanaga S. Microtubule-stimulated phosphorylation of tau at Ser202 and Thr205 by cdk5 decreases its microtubule nucleation activity. J Biochem. 1998; 124:738–46. [PubMed: 9756618]

West AE, Neve RL, Buckley KM. Targeting of the synaptic vesicle protein synaptobrevin in the axon of cultured hippocampal neurons: evidence for two distinct sorting steps. J Cell Biol. 1997; 139:917–27. [PubMed: 9362510]

White JG, Southgate E, Thomson JN, Brenner S. The structure of the nervous system of *Caenorhabditis elegans*. Philos Trans R Soc Lond B Biol Sci. 1986; 314:1–340. [PubMed: 22462104]

Yoder JH, Han M. Cytoplasmic dynein light intermediate chain is required for discrete aspects of mitosis in *Caenorhabditis elegans*. Mol Biol Cell. 2001; 12:2921–33. [PubMed: 11598181]

Zahn TR, Angleson JK, MacMorris MA, Domke E, Hutton JF, Schwartz C, Hutton JC. Dense core vesicle dynamics in *Caenorhabditis elegans* neurons and the role of kinesin UNC-104. Traffic. 2004; 5:544–59. [PubMed: 15180830]

Zheng Y, Wildonger J, Ye B, Zhang Y, Kita A, Younger SH, Zimmerman S, Jan LY, Jan YN. Dynein is required for polarized dendritic transport and uniform microtubule orientation in axons. Nat Cell Biol. 2008; 10:1172–80. [PubMed: 18758451]

Zhou HM, Brust-Mascher I, Scholey JM. Direct visualization of the movement of the monomeric axonal transport motor UNC-104 along neuronal processes in living *Caenorhabditis elegans*. J Neurosci. 2001; 21:3749–55. [PubMed: 11356862]

Zhou KM, Dong YM, Ge Q, Zhu D, Zhou W, Lin XG, Liang T, Wu ZX, Xu T. PKA activation bypasses the requirement for UNC-31 in the docking of dense core vesicles from *C. elegans* neurons. Neuron. 2007; 56:657–69. [PubMed: 18031683]

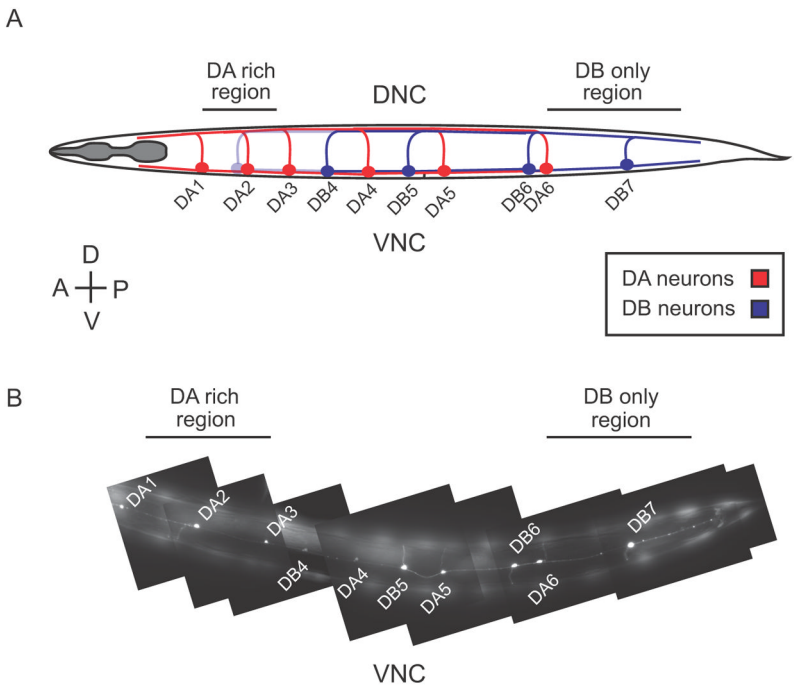

Figure 1. The *unc-129* promoter controls expression in a subset of DA and DB motor neurons

(A) Schematic diagram of DA and DB motor neurons under the control of the *unc-129* promoter used in this study. DA and DB neurons have cell bodies located on the ventral side with dendrites in the VNC and axons in the DNC. DA neurons (red) project their processes towards the anterior, whereas DB neurons (blue) project their processes towards the posterior. The DA rich and DB only regions of the VNC and DNC imaged throughout this study are indicated. (B) A photomontage of the VNC of transgenic animals expressing soluble mCherry under the control of the *unc-129* promoter. Specific DA and DB neuron cell bodies and processes expressing mCherry are shown. Neuron identities were determined based on the position of their cell bodies and the projections of their commissures. Strong mCherry expression was observed in DA1–6 and DB4–7, whereas occasional, weak expression was seen in DB3, whose cell body is located just anterior to DA2 (see (A)). To isolate fluorescent signals derived only from DB neurons, neuronal processes were imaged in regions of the VNC and DNC posterior to the DA6 cell body (DB only region). To enrich for fluorescent signals derived from DA neurons, processes were imaged in regions of the VNC and DNC anterior to the DA3 cell body (DA rich region). The animals are oriented with anterior to the left and dorsal to the top.

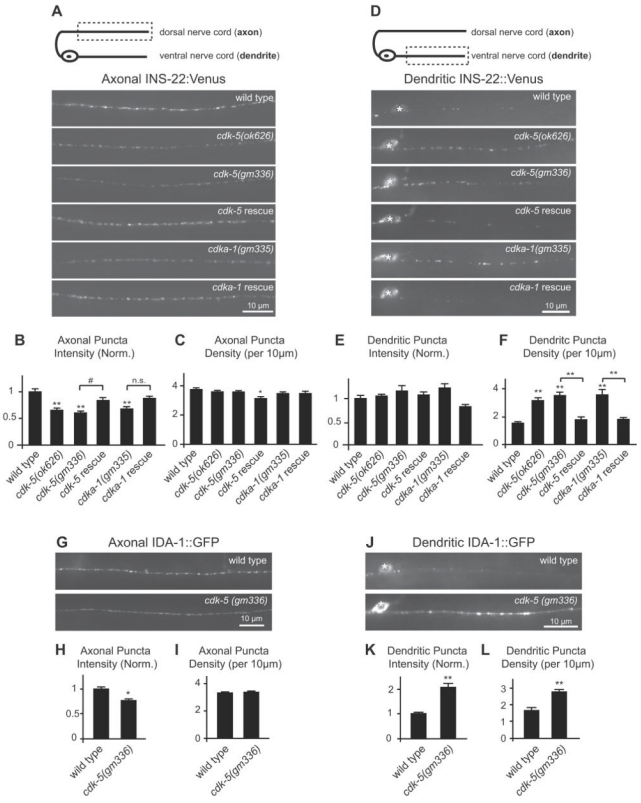

Figure 2. CDK-5 regulates the polarized distribution of DCVs in DB motor neurons

(A) Schematic diagram of a DB motor neuron with axon in the dorsal nerve cord (DNC) and dendrite in the ventral nerve cord (VNC)(top panel). This diagram is oriented with the anterior of the animal to the left for this and all subsequent figures. The boxed region denotes that the axon was imaged for data presented in panels (A–C, G–I). Representative images of INS-22::Venus in DB axons of young adult wild-type, *cdk-5(ok626)*, *cdk-5(gm336)*, *Punc-129::cdk-5;cdk-5(gm336)* rescue, *cdka-1(gm335)*, and *Punc-129::cdka-1;cdka-1(gm335)* rescue animals (bottom panels). (B–C) Quantification of INS-22::Venus puncta intensity (B) and density (C) in axons of wild-type (n=30), *cdk-5(ok626)*(n=25), *cdk-5(gm336)*(n=35), *cdk-5* rescue (n=19), *cdka-1(gm335)*(n=23), and *cdka-1* rescue (n=20) animals. (D) Schematic diagram of a DB motor neuron (top panel). The boxed region denotes that the dendrite was imaged for data presented in panels (D–F, J–L). Representative images of INS-22::Venus in DB dendrites of wild-type, *cdk-5(ok626)*, *cdk-5(gm336)*, *Punc-129::cdk-5;cdk-5(gm336)* rescue, *cdka-1(gm335)*, and *Punc-129::cdka-1;cdka-1(gm335)* rescue animals are shown. For this and all other dendrite images, the white asterisk (*) indicates the position of a motor neuron cell body. (E–F) Quantification of INS-22::Venus puncta intensity (E) and density (F) in dendrites of wild-type (n=27), *cdk-5(ok626)*(n=19), *cdk-5(gm336)*(n=19), *cdk-5* rescue (n=19), *cdka-1(gm335)*(n=15), and *cdka-1* rescue (n=18) animals. (G) Representative images of IDA-1::GFP in DB axons of young adult wild type and *cdk-5(gm336)* mutant animals. (H–I) Quantification of IDA-1::GFP puncta intensity (H) and density (I) in axons of wild-type (n=27) and *cdk-5(gm336)*(n=25) mutant animals. (J) Representative images of IDA-1::GFP in DB dendrites of wild type and *cdk-5(gm336)* mutant animals. (K–L) Quantification of IDA-1::GFP puncta intensity (K) and density (L) in dendrites of wild-type (n=23) and *cdk-5(gm336)*(n=25) mutant animals. For this and all subsequent figures, error bars denote standard error from the mean (SEM). Values that differ significantly (Tukey-Kramer (B, C, E, and F) and Student's *t* test (H, I, K, and L)) from wild type (marked by asterisks above

each bar) or from other genotypes (comparisons marked by brackets) are denoted on the graphs (#$p<0.05$, *$p<0.01$, **$p<0.001$) and values that do not differ significantly ($p>0.05$) are denoted by n.s.

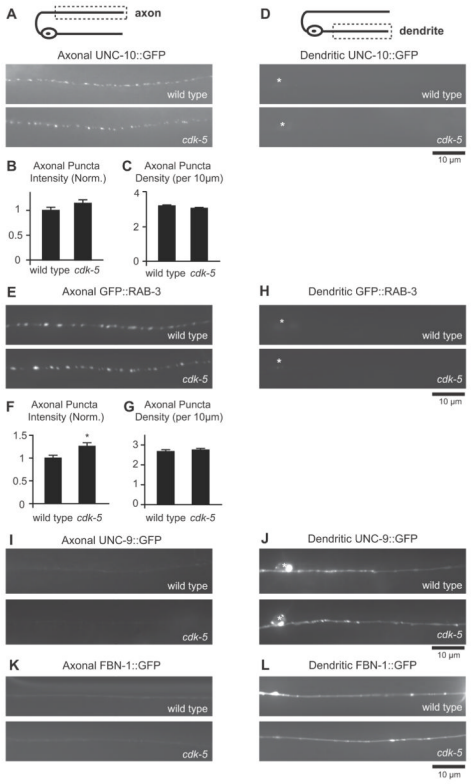

Figure 3. The polarized distribution of axonal and dendritic markers in DB motor neurons is not affected in *cdk-5* mutants

(A) Schematic diagram of a DB motor neuron (top panel). The boxed region denotes that the axon was imaged for data presented in panels (A–C, E–G, I and K). Representative images of UNC-10::GFP in DB axons of wild-type and *cdk-5* mutant animals (bottom panels). (B–C) Quantification of UNC-10::GFP puncta intensity (B) and density (C) in axons of wild-type (n=21) and *cdk-5(gm336)*(n=20) mutant animals. (D) Schematic diagram of a DB motor neuron (top panel). The boxed region denotes that the dendrite was imaged for data presented in panels (D, H, J and L). Representative images of UNC-10::GFP in DB dendrites of wild type and *cdk-5(gm336)* mutant animals (bottom panels). (E) Representative images of GFP::RAB-3 in DB axons of wild-type and *cdk-5(gm336)* mutant animals. (F–G) Quantification of GFP::RAB-3 puncta intensity (F) and density (G) in axons of wild-type (n=22) and *cdk-5(gm336)*(n=21) mutant animals. (H) Representative images of GFP::RAB-3 in DB dendrites of wild-type and *cdk-5(gm336)* mutant animals. Values that differ significantly from wild type (Student's *t* test) are denoted on graphs (*p<0.01). (I) Representative images of UNC-9::GFP in DB axons of wild-type and *cdk-5(gm336)* mutant animals. (J) Representative images of UNC-9::GFP in DB dendrites of wild-type and *cdk-5(gm336)* mutant animals. (K) Representative images of FBN-1::GFP in DB axons of wild-type and *cdk-5(gm336)* mutant animals. (L) Representative images of FBN-1::GFP in DB dendrites of wild-type and *cdk-5(gm336)* mutant animals.

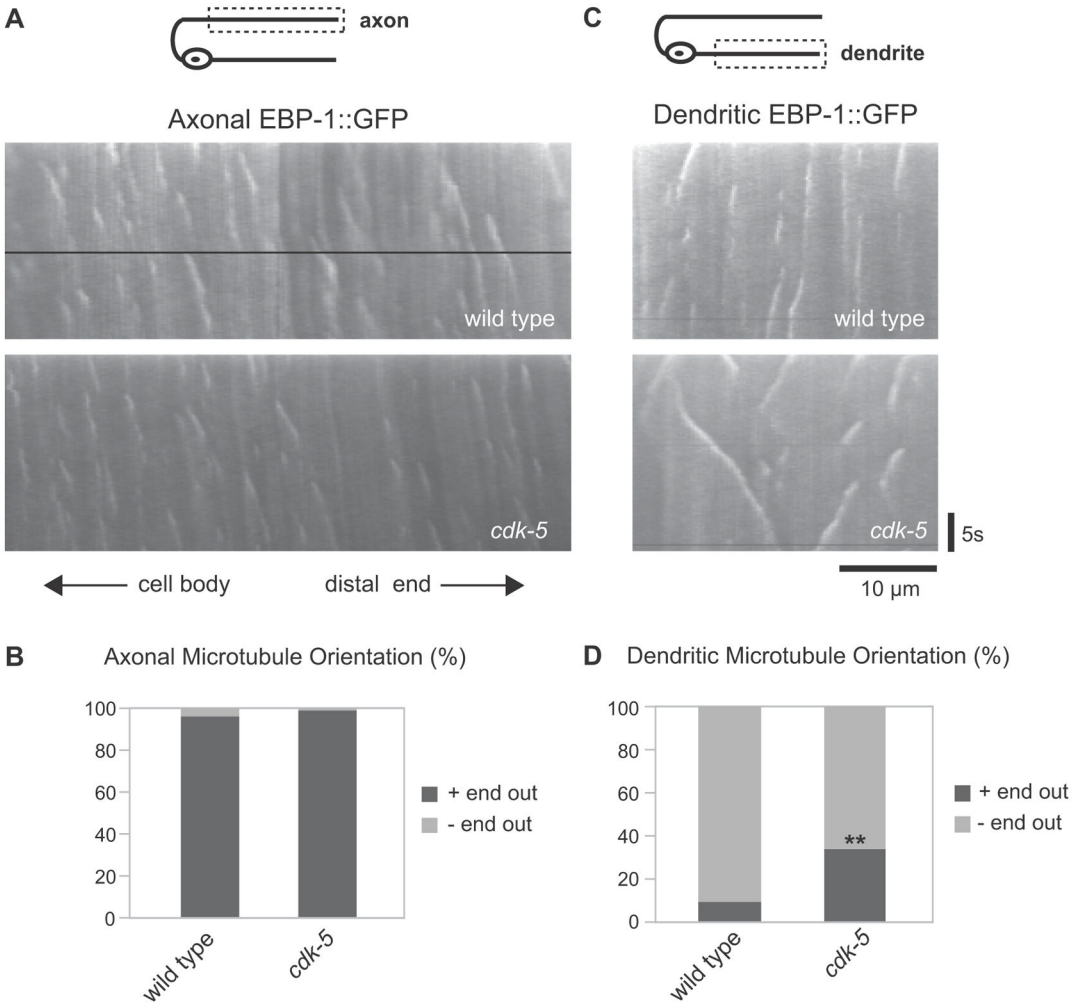

Figure 4. CDK-5 regulates the orientation of microtubules in DB dendrites

(A) Schematic diagram of a DB motor neuron (top panel). The boxed region denotes that the axon was imaged for data presented in panels (A–B). Representative kymographs generated from a 25 second movie of EBP-1::GFP movement in the axon of wild type and *cdk-5(gm336)* mutant animals (bottom panels). (B) Quantification of percent plus-end and minus-end out microtubules in wild type (n=76 puncta) and *cdk-5* (n=93 puncta) mutant animals based on analysis of EBP-1::GFP movement in DB axons. (C) Schematic diagram of a DB motor neuron (top panel). The boxed region denotes that the dendrite was imaged for data presented in panels (C–D). Representative kymographs generated from a 25 second movie of EBP-1::GFP movement in the dendrite of wild type and *cdk-5(gm336)* mutant animals (bottom panels). (D) Quantification of percent plus-end and minus-end out microtubules in wild type (n=107 puncta) and *cdk-5* (n=195 puncta) mutant animals based on analysis of EBP-1::GFP movement in DB dendrites. Values that differ significantly from wild type (Chi-square test, Yates' correction) are denoted on the graphs (**p<0.001).

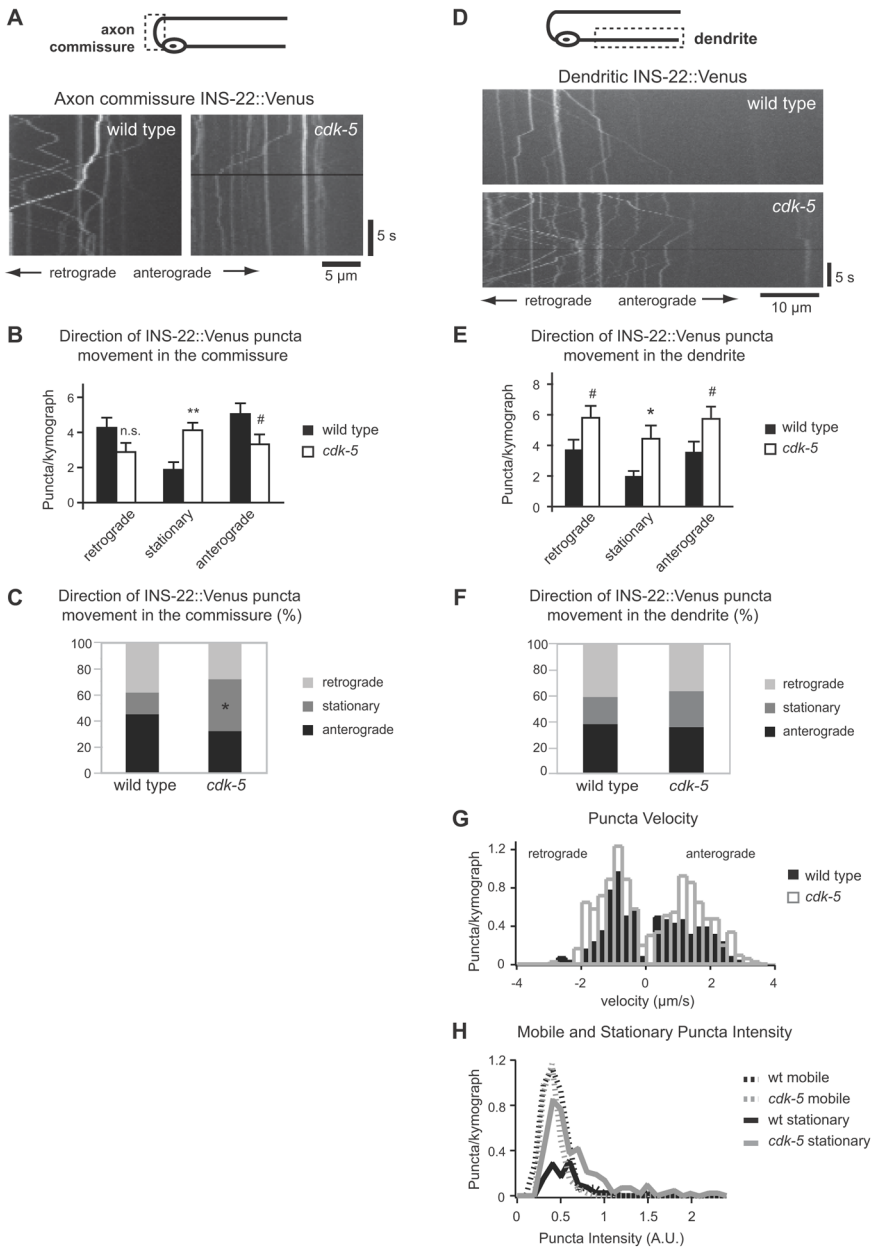

Figure 5. CDK-5 regulates DCV trafficking in DB motor neuron axons and dendrites

(A) Schematic diagram of a DB motor neuron (top panel). The boxed region denotes that the axon commissure was imaged for data presented in panels (A–C). Representative kymographs generated from 20s movies of INS-22::Venus puncta movement in DB axon commissures of wild type and *cdk-5(gm336)* mutant animals (bottom panels). (B) Quantification of the average number of INS-22::Venus puncta moving anterogradely, retrogradely, or remaining stationary in each kymograph from wild type (n=23) and *cdk-5* (n=25) mutant axon commissures. (C) Quantification of the direction of INS-22::Venus puncta movement as a percentage of total puncta, in wild type (n=257 puncta) and *cdk-5* (n=258) mutant axon commissures. (D) Schematic diagram of a DB motor neuron (top panel). The boxed region denotes that the dendrite was imaged for data presented in panels (D–H). Representative kymographs generated from 20s movies of INS-22::Venus

movement in DB dendrites of wild type and *cdk-5(gm336)* mutant animals (bottom panels). (E) Quantification of the average number of INS-22::Venus puncta moving anterogradely, retrogradely, or remaining stationary in each kymograph from wild type (n=26) and *cdk-5* (n=29) mutant dendrites. (F) Quantification of the direction of INS-22::Venus puncta movement, as a percentage of total puncta, in wild type (n=238 puncta) and *cdk-5* (n=479) mutant dendrites. (G) Histogram of INS-22::Venus puncta velocities in dendrites of wild type and *cdk-5* mutant animals. Positive velocities represent anterograde movements and negative velocities represent retrograde movements. (H) Histogram of mobile and stationary INS-22::Venus puncta intensity in dendrites of wild type and *cdk-5* mutant animals. Values that differ significantly (Student's *t* test (B and E) and Chi-Square test (C)) from wild type are denoted on graphs (**p<0.001, *p<0.01, #p<0.05).

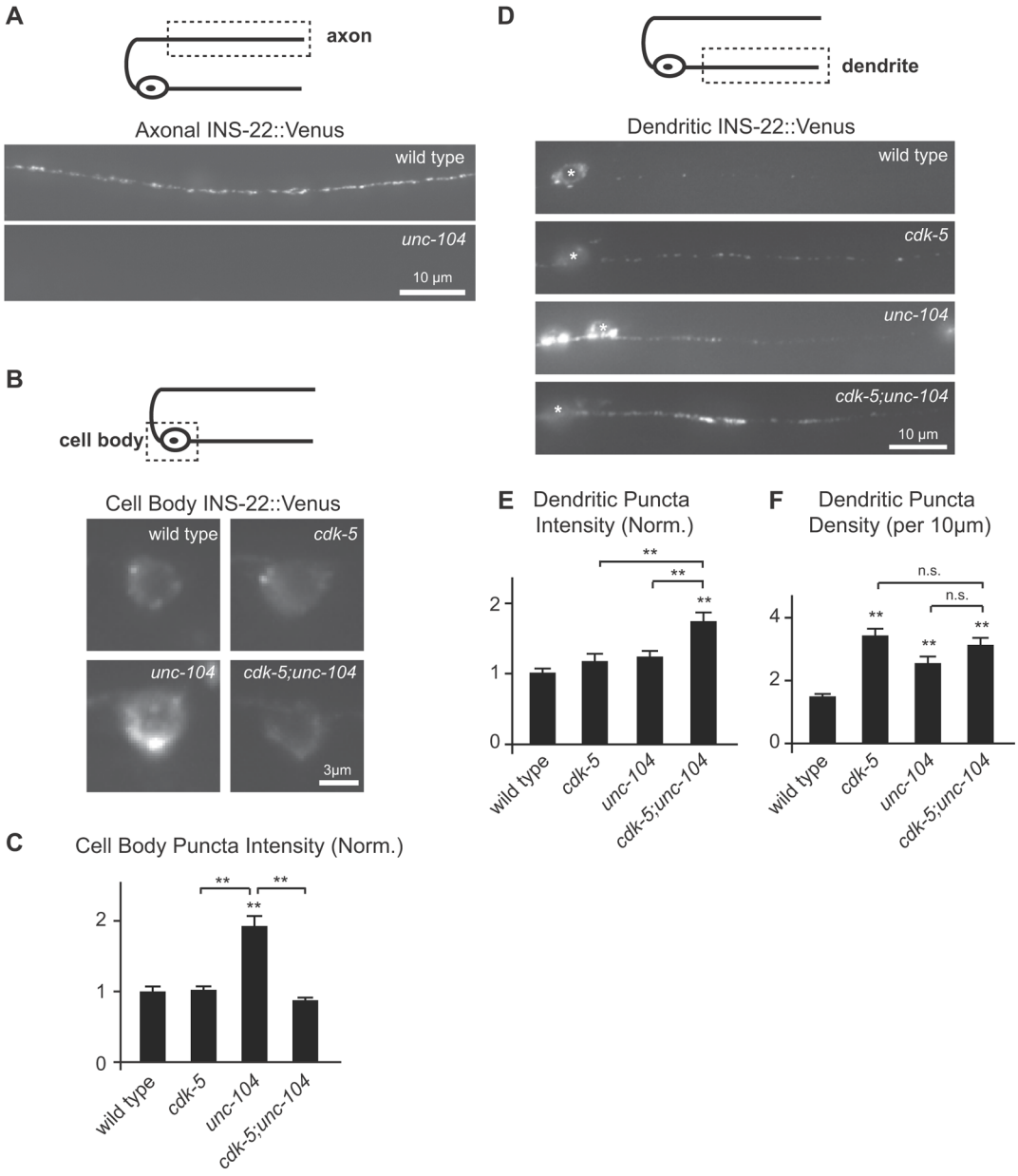

Figure 6. UNC-104/Kif1A is not required for the increase in dendritic DCVs in *cdk-5* mutants

(A) Schematic diagram of a DB motor neuron (top panel). The boxed region denotes that the axon was imaged for data presented in panel (A). Representative images of INS-22::Venus in DB axons of wild type and *unc-104(e1265)* mutant animals (bottom panels). (B) Schematic diagram of a DB motor neuron (top panel). The boxed region denotes that the cell body was imaged for data presented in panels (B–C). Representative images of INS-22::Venus in the DB6 motor neuron cell body of wild type, *cdk-5(gm336)*, *unc-104(e1265)*, and *cdk-5;unc-104* double mutant animals (bottom panels). (C) Quantification of INS-22::Venus fluorescence intensity in DB cell bodies of wild-type (n=24), *cdk-5* (n=14), *unc-104* (n=11), and *cdk-5;unc-104* (n=14) double mutant animals. (D) Schematic diagram of a DB motor neuron (top panel). The boxed region denotes that the dendrite was imaged for data presented in panels (D–F). Representative images of INS-22::Venus in DB dendrites of wild-type, *cdk-5(gm336)*, *unc-104(e1256)*, and

cdk-5;unc-104 double mutant animals (bottom panels). (E–F) Quantification of INS-22::Venus puncta intensity (E) and density (F) in DB dendrites of wild-type (n=27), *cdk-5* (n=19), *unc-104* (n=18), and *cdk-5;unc-104* (n=18) animals. Values that differ significantly (Tukey-Kramer test) from wild type (marked by asterisks above each bar) or from other genotypes (comparisons marked by brackets) are denoted on the graphs (**$p<0.001$, n.s. $p>0.05$).

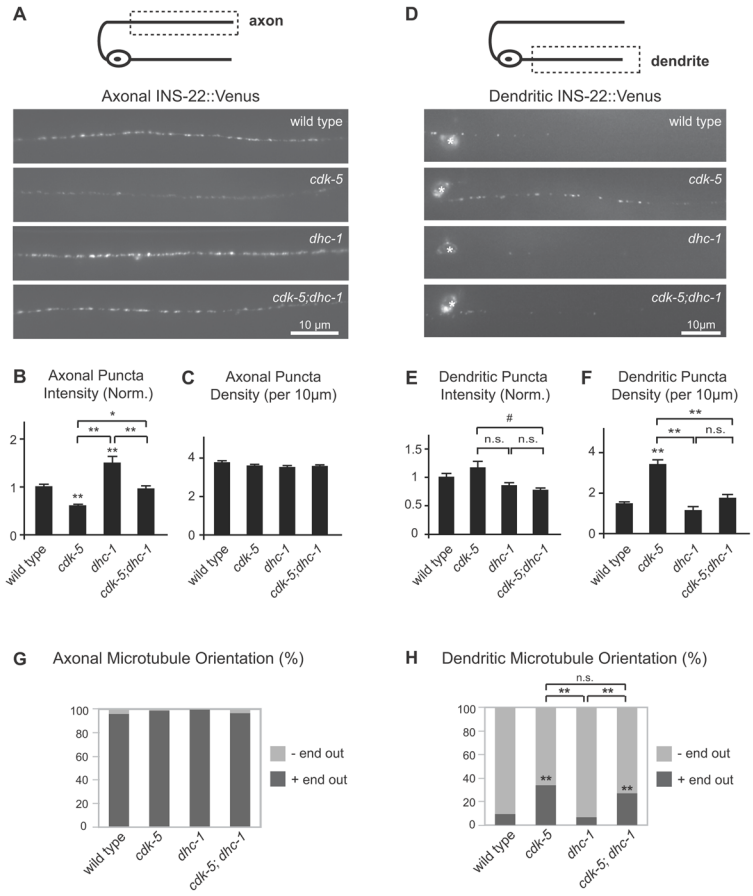

Figure 7. Cytoplasmic dynein is required for the increase in dendritic DCVs in *cdk-5* mutant DB dendrites

(A) Schematic diagram of a DB motor neuron (top panel). The boxed region denotes that the axon was imaged for data presented in panels (A–C, G). Representative images of INS-22::Venus DB axons of wild type, *cdk-5(gm336)*, *dhc-1(js319)*, and *cdk-5;dhc-1* double mutant animals (bottom panels). (B–C) Quantification of INS-22::Venus puncta intensity (B) and density (C) in axons of wild type (n=30), *cdk-5* (n=35), *dhc-1* (n=22), *cdk-5;dhc-1* (n=20) animals. (D) Schematic diagram of a DB motor neuron (top panel). The boxed region denotes that the dendrite was imaged for data presented in panels (D–F, H). Representative images of INS-22::Venus in DB dendrites of wild type, *cdk-5(gm336)*, *dhc-1(js319)*, and *cdk-5;dhc-1* double mutant animals (bottom panels). (E–F) Quantification of INS-22::Venus puncta intensity (E) and density (F) in dendrites of wild type (n=27), *cdk-5* (n=19), *dhc-1* (n=12), *cdk-5;dhc-1* (n=19) animals. (G) Quantification of percent plus-end out and minus-end out microtubules in DB axons of wild type (n=76 puncta), *cdk-5(gm336)*(n=93), *dhc-1(js319)*(n=36), and *cdk-5;dhc-1*(n=61) double mutants based on analysis of EBP-1::GFP movement in axons. (H) Quantification of percent plus-end out and minus-end out microtubules in DB dendrites of wild type (n=107 puncta), *cdk-5(gm336)*(n=195), *dhc-1(js319)*(n=60), and *cdk-5;dhc-1* (n=218) double mutant animals based on analysis of EBP-1::GFP movement in dendrites. Values that differ significantly (Tukey-Kramer test (B, C, E, and F) and Chi-Square test (G and H)) from wild type (marked by asterisks above each bar) or from other genotypes (comparisons marked by brackets) are denoted on the graphs (**p<0.001, *p<0.01, #p<0.05, n.s. p>0.05).

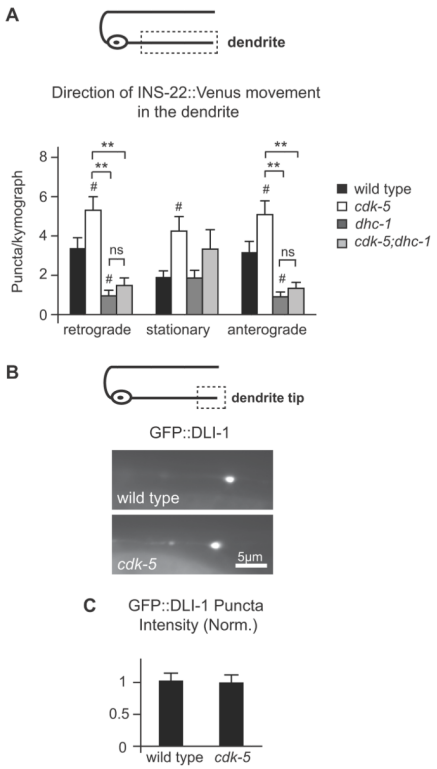

Figure 8. Cytoplasmic dynein is required for DCV trafficking in DB motor neuron dendrites in wild type and *cdk-5* mutant animals

(A) Schematic diagram of a DB motor neuron (top panel). The boxed region denotes that the dendrite was imaged for data presented in panel (A). Quantification of the direction of INS-22::Venus puncta movement in DB dendrites of wild-type (n=34), *cdk-5(gm336)* (n=36), *dhc-1(js319)*(n=21) and *cdk-5;dhc-1* (n=29) double mutant dendrites (bottom panel). (B) Schematic diagram of a DB motor neuron (top panel). The boxed region denotes that the distal dendrite tip was imaged for data presented in panels (B–C). Representative images of GFP::DLI-1 accumulations at the distal tip of DB7 dendrites in wild-type and *cdk-5(gm336)* mutant animals (bottom panels). (C) Quantification of GFP::DLI-1 puncta intensity at the tip of DB7 dendrites in wild-type (n=29) and *cdk-5* (n=23) mutant animals. Values that differ significantly (Tukey-Kramer test) from wild type (marked by symbols above each bar) or from other genotypes (comparisons marked by brackets) are denoted on the graphs (**p<0.001, #p<0.05, n.s. p>0.05).